High-redshift Quasars, Clusters of Galaxies, and Large-scale Structure: Scientific Discoveries and Opportunities with the Sloan Digital Sky Survey

Michael A. Strauss, for the SDSS Collaboration

(Chicago, Fermilab, IAS, Japan Promotion Group, John Hopkins, Princeton, USNO, NMSU, U. Washington, MPA, MPIA)

- Overview of the Survey
- Selection of quasars at low and high redshift
- The nature of quasars at high redshift
- The Quasar Luminosity Function
- Brown Dwarfs
- Mystery Objects
- Clusters of Galaxies
- Structure of the Galactic Halo

THE ASTRONOMICAL JOURNAL, 120:1579–1587, 2000 September

The SDSS is a big Collaboration!

THE SLOAN DIGITAL SKY SURVEY: TECHNICAL SUMMARY

DONALD G. YORK,[1] J. ADELMAN,[2] JOHN E. ANDERSON, JR.,[2] SCOTT F. ANDERSON,[3] JAMES ANNIS,[2] NETA A. BAHCALL,[4] J. A. BAKKEN,[2] ROBERT BARKHOUSER,[5] STEVEN BASTIAN,[2] EILEEN BERMAN,[2] WILLIAM N. BOROSKI,[2] STEVE BRACKER,[2] CHARLIE BRIEGEL,[2] JOHN W. BRIGGS,[6] J. BRINKMANN,[7] ROBERT BRUNNER,[8] SCOTT BURLES,[1] LARRY CAREY,[3] MICHAEL A. CARR,[4] FRANCISCO J. CASTANDER,[1,9] BING CHEN,[5] PATRICK L. COLESTOCK,[2] A. J. CONNOLLY,[10] J. H. CROCKER,[5] ISTVÁN CSABAI,[5,11] PAUL C. CZARAPATA,[2] JOHN ERIC DAVIS,[7] MAMORU DOI,[12] TOM DOMBECK,[1] DANIEL EISENSTEIN,[1,13,14] NANCY ELLMAN,[15] BRIAN R. ELMS,[4,16] MICHAEL L. EVANS,[3] XIAOHUI FAN,[4] GLENN R. FEDERWITZ,[2] LARRY FISCELLI,[1] SCOTT FRIEDMAN,[5] JOSHUA A. FRIEMAN,[1,2] MASATAKA FUKUGITA,[13,17] BRUCE GILLESPIE,[7] JAMES E. GUNN,[4] VIJAY K. GURBANI,[2] ERNST DE HAAS,[4] MERLE HALDEMAN,[2] FREDERICK H. HARRIS,[18] J. HAYES,[7] TIMOTHY M. HECKMAN,[5] G. S. HENNESSY,[19] ROBERT B. HINDSLEY,[20] SCOTT HOLM,[2] DONALD J. HOLMGREN,[2] CHI-HAO HUANG,[2] CHARLES HULL,[21] DON HUSBY,[2] SHIN-ICHI ICHIKAWA,[16] TAKASHI ICHIKAWA,[22] ŽELJKO IVEZIĆ,[4] STEPHEN KENT,[2] RITA S. J. KIM,[4] E. KINNEY,[7] MARK KLAENE,[7] A. N. KLEINMAN,[7] S. KLEINMAN,[7] G. R. KNAPP,[4] JOHN KORIENEK,[2] RICHARD G. KRON,[1,2] PETER Z. KUNSZT,[5] D. Q. LAMB,[1] B. LEE,[2] R. FRENCH LEGER,[3] SIRILUK LIMMONGKOL,[3] CARL LINDENMEYER,[2] DANIEL C. LONG,[7] CRAIG LOOMIS,[7] JON LOVEDAY,[1] RICH LUCINIO,[7] ROBERT H. LUPTON,[4] BRYAN MACKINNON,[2,23] EDWARD J. MANNERY,[3] P. M. MANTSCH,[2] BRUCE MARGON,[3] PEREGRINE MCGEHEE,[24] TIMOTHY A. MCKAY,[25] AVERY MEIKSIN,[26] ARONNE MERELLI,[27] DAVID G. MONET,[18] JEFFREY A. MUNN,[18] VIJAY K. NARAYANAN,[4] THOMAS NASH,[2] ERIC NEILSEN,[5] RICH NESWOLD,[2] HEIDI JO NEWBERG,[2,28] R. C. NICHOL,[27] TOM NICINSKI,[2,29] MARIO NONINO,[30] NORIO OKADA,[16] SADANORI OKAMURA,[12] JEREMIAH P. OSTRIKER,[4] RUSSELL OWEN,[3] A. GEORGE PAULS,[4] JOHN PEOPLES,[2] R. L. PETERSON,[2] DONALD PETRAVICK,[2] JEFFREY R. PIER,[18] ADRIAN POPE,[27] RUTH PORDES,[2] ANGELA PROSAPIO,[2] RON RECHENMACHER,[2] THOMAS R. QUINN,[3] GORDON T. RICHARDS,[1] MICHAEL W. RICHMOND,[31] CLAUDIO H. RIVETTA,[2] CONSTANCE M. ROCKOSI,[1] KURT RUTHMANSDORFER,[2] DALE SANDFORD,[6] DAVID J. SCHLEGEL,[4] DONALD P. SCHNEIDER,[32] MAKI SEKIGUCHI,[17] GARY SERGEY,[2] KAZUHIRO SHIMASAKU,[12] WALTER A. SIEGMUND,[3] STEPHEN SMEE,[5] J. ALLYN SMITH,[25] S. SNEDDEN,[7] R. STONE,[18] CHRIS STOUGHTON,[2] MICHAEL A. STRAUSS,[4] CHRISTOPHER STUBBS,[3] MARK SUBBARAO,[1] ALEXANDER S. SZALAY,[5] ISTVAN SZAPUDI,[33] GYULA P. SZOKOLY,[5] ANIRUDDA R. THAKAR,[5] CHRISTY TREMONTI,[5] DOUGLAS L. TUCKER,[2] ALAN UOMOTO,[5] DAN VANDEN BERK,[2] MICHAEL S. VOGELEY,[34] PATRICK WADDELL,[3] SHU-I WANG,[1] MASARU WATANABE,[35] DAVID H. WEINBERG,[36] BRIAN YANNY,[2] AND NAOKI YASUDA[16]
(THE SDSS COLLABORATION)

Received 2000 February 13; accepted 2000 June 8

ABSTRACT

The Sloan Digital Sky Survey (SDSS) will provide the data to support detailed investigations of the distribution of luminous and nonluminous matter in the universe: a photometrically and astrometrically calibrated digital imaging survey of π sr above about Galactic latitude 30° in five broad optical bands to a depth of $g' \sim 23$ mag, and a spectroscopic survey of the approximately 10^6 brightest galaxies and 10^5 brightest quasars found in the photometric object catalog produced by the imaging survey. This paper summarizes the observational parameters and data products of the SDSS and serves as an introduction to extensive technical on-line documentation.

Key words: cosmology: observations — instrumentation: miscellaneous

[1] Department of Astronomy and Astrophysics, University of Chicago, 5640 South Ellis Avenue, Chicago, IL 60637.
[2] Fermi National Accelerator Laboratory, P.O. Box 500, Batavia, IL 60510.
[3] Department of Astronomy, University of Washington, Box 351580, Seattle, WA 98195.
[4] Princeton University Observatory, Peyton Hall, Princeton, NJ 08544-1001.
[5] Department of Physics and Astronomy, Johns Hopkins University, 3400 North Charles Street, Baltimore, MD 21218-2686.
[6] Yerkes Observatory, University of Chicago, 373 West Geneva Street, Williams Bay, WI 53191.
[7] Apache Point Observatory, P.O. Box 59, Sunspot, NM 88349.
[8] Department of Astronomy, 105-24, California Institute of Technology, 1201 East California Boulevard, Pasadena, CA 91125.
[9] Observatoire Midi-Pyrénées, 14 avenue Edouard Belin, F-31400 Toulouse, France.
[10] Department of Physics and Astronomy, University of Pittsburgh, 3941 O'Hara Street, Pittsburgh, PA 15260.
[11] Department of Physics of Complex Systems, Eötvös University, Pázmány Péter sétány 1/A, H-1117 Budapest, Hungary.
[12] Department of Astronomy and Research Center for the Early Universe, School of Science, University of Tokyo, 7-3-1 Hongo, Bunkyo, Tokyo 113-0033, Japan.
[13] Institute for Advanced Study, Olden Lane, Princeton, NJ 08540-0631.
[14] Hubble Fellow.
[15] Department of Physics, Yale University, P.O. Box 208121, New Haven, CT 06520.
[16] National Astronomical Observatory, 2-21-1 Osawa, Mitaka, Tokyo 181-8588, Japan.
[17] Institute for Cosmic Ray Research, University of Tokyo, 3-2-1 Midori, Tanashi, Tokyo 188-8502, Japan.
[18] US Naval Observatory, Flagstaff Station, P.O. Box 1149, Flagstaff, AZ 86002.
[19] US Naval Observatory, 3450 Massachusetts Avenue, NW, Washington, DC 20392-5420.
[20] Remote Sensing Division, Code 7215, Naval Research Laboratory, 4555 Overlook Avenue, SW, Washington, DC 20375.
[21] Observatories of the Carnegie Institution of Washington, 813 Santa Barbara Street, Pasadena, CA 91101.
[22] Astronomical Institute, Tohoku University, Aramaki, Aoba, Sendai 980-8578, Japan.

Scientific Goals:

- A proper accounting of the nature of objects in the local universe
- Large-Scale Structure from < 1 Mpc to 300 Mpc and beyond
- Galaxy Clustering of different types of galaxies
- Catalog of Clusters of Galaxies to $z = 0.5$; the evolution thereof
- The Multivariate Manifold of Galaxies
- Faint galaxy counts and photometric redshifts
- Large-Scale Distribution of Quasars
- The Evolution of Quasars
- Large-Scale Structure from Quasar Absorption Lines
- Star counts and populations; Structure of the Galaxy
- Reddening map over the survey area
- Serendipity!

Sloan Digital Sky Survey

- Five band imaging, 3000-10,000Å, over 1/4 of Celestial Sphere, to 23rd mag. Images of order 10^8 stars and galaxies.
- Follow-up spectroscopy of 10^6 galaxies and 10^5 quasars.

Hardware

Primary Telescope	Wide-Field (2.5°) 2.5m R-C, f/5.0
Photometric Telescope	20-inch telescope, 1° FOV
Imaging Camera	30 2048 × 2048 CCD's +
	24 2048 × 400 CCD's
Data Rate	5 Mbytes/second = 20 Gbytes/hour
	20 square degrees/hour
Two Spectrographs	Fiber-fed, with red and blue cameras
Fiber System	Plug plates, 640 fibers with 3″ aperture

Imaging Survey: North

Scan at Sidereal Rate	Exposure Time of 54 sec
Sky Coverage	10,000 square degrees (28% covered twice
Passbands	u (3550Å), g (4685Å), r (6165Å), i (7480Å), z (8930Å)
Resolution	$1 - 1.5$ arcsec
Positional Accuracy	0.10 arcsec
Depth	$u = 22.0, g = 22.2, r = 22.2$, $i = 21.3, z = 20.5$
Photometric Calibration	Aiming for 2%

SDSS CAMERA

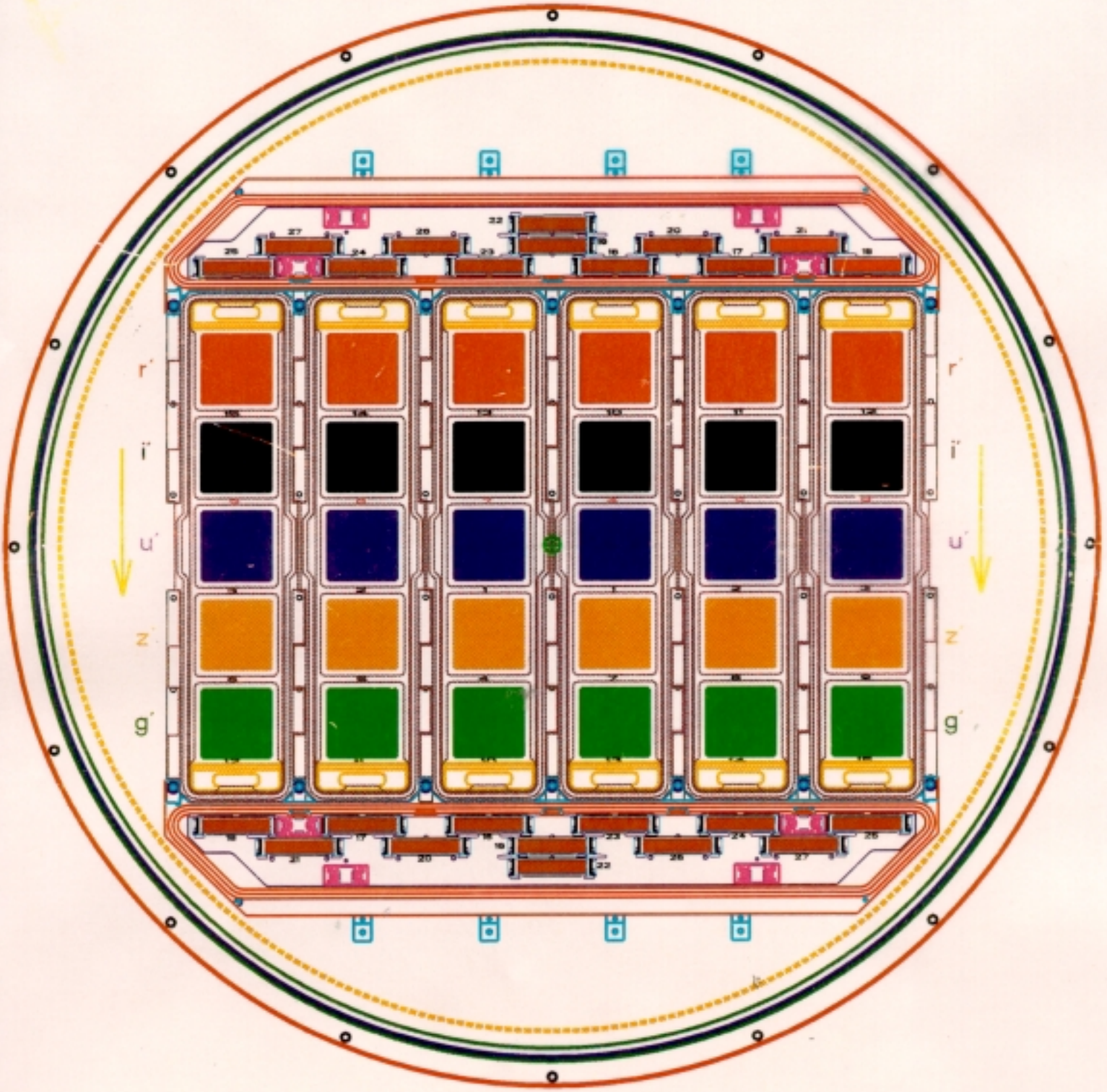

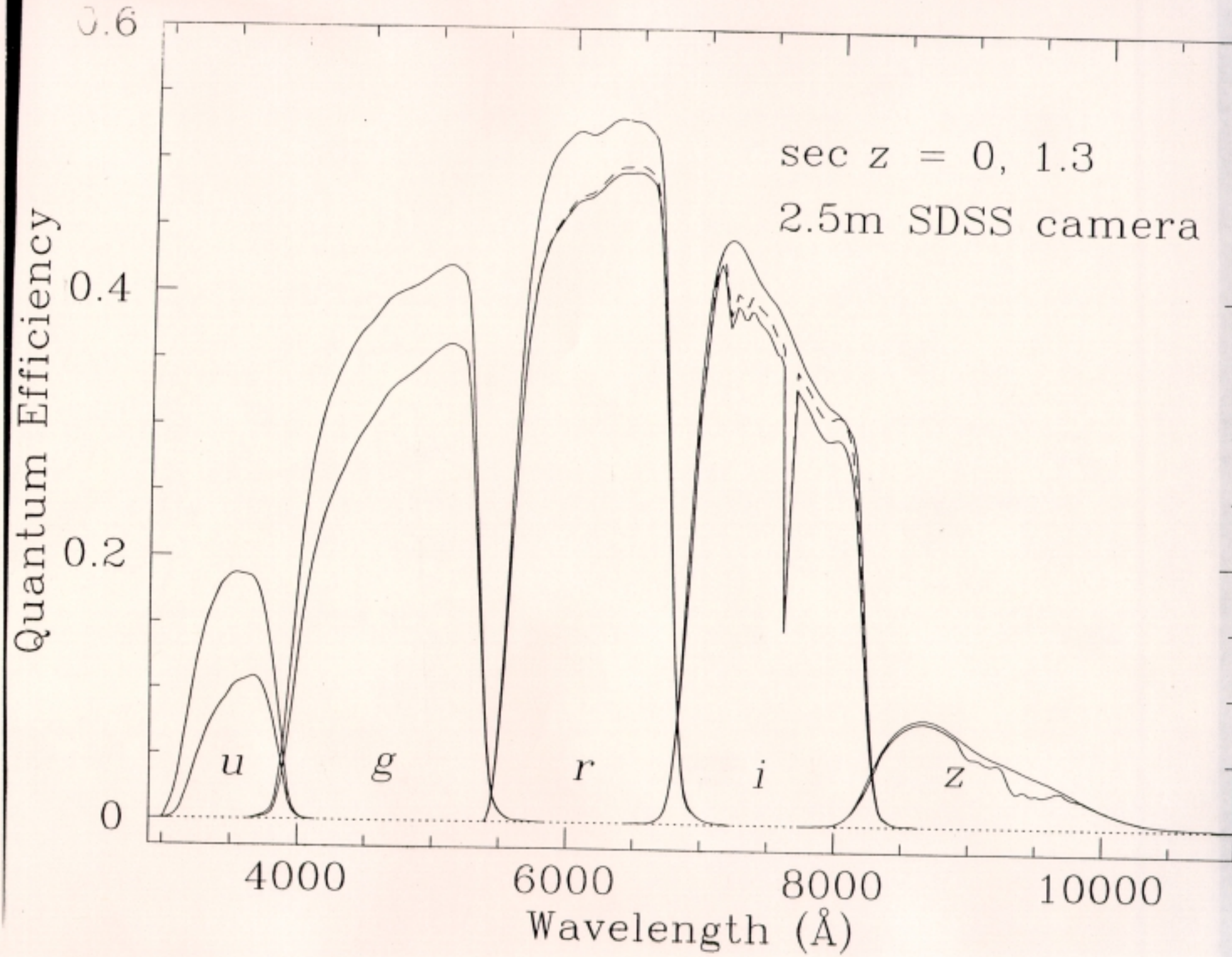
0.6
0.4
0.2
0
Quantum Efficiency
sec z = 0, 1.3
2.5m SDSS camera
u
g
r
i
z
4000
6000
8000
10000
Wavelength (Å)

Imaging Survey: Southern Galactic Cap

Sky Coverage	≈ 200 square degrees at $\delta = 0°$
Depth	Two magnitudes deeper
# of Exposures	≈ 40

Spectroscopic Survey

Exposure Time	45 minutes
Coverage	3800-9200Å= 4096 pixels
Resolution	$R = 2000$ (2.5Å= 2 pixels at 5000 Å)
Throughput	28% at peak
Galaxies	10^6 with $r < 17.7$, LSS at $0 < z < 0.2$
	10^5 luminous red ellipticals with $r < 19.5$; $z \leq 0.4$
Quasars	10^5, selected by colors; $i < 19.1$, $0 < z < 5.5$

Also miscellaneous stars, radio and X-ray sources, etc.

Schedule

First-light imaging	May 1998
First-light spectroscopy	June 1999
Routine operations	April 2000
First Public Data Release	June 2001

Over 2000 square degrees of imaging data thus far, and spectra of 200,000 objects.

SDSS Spectra

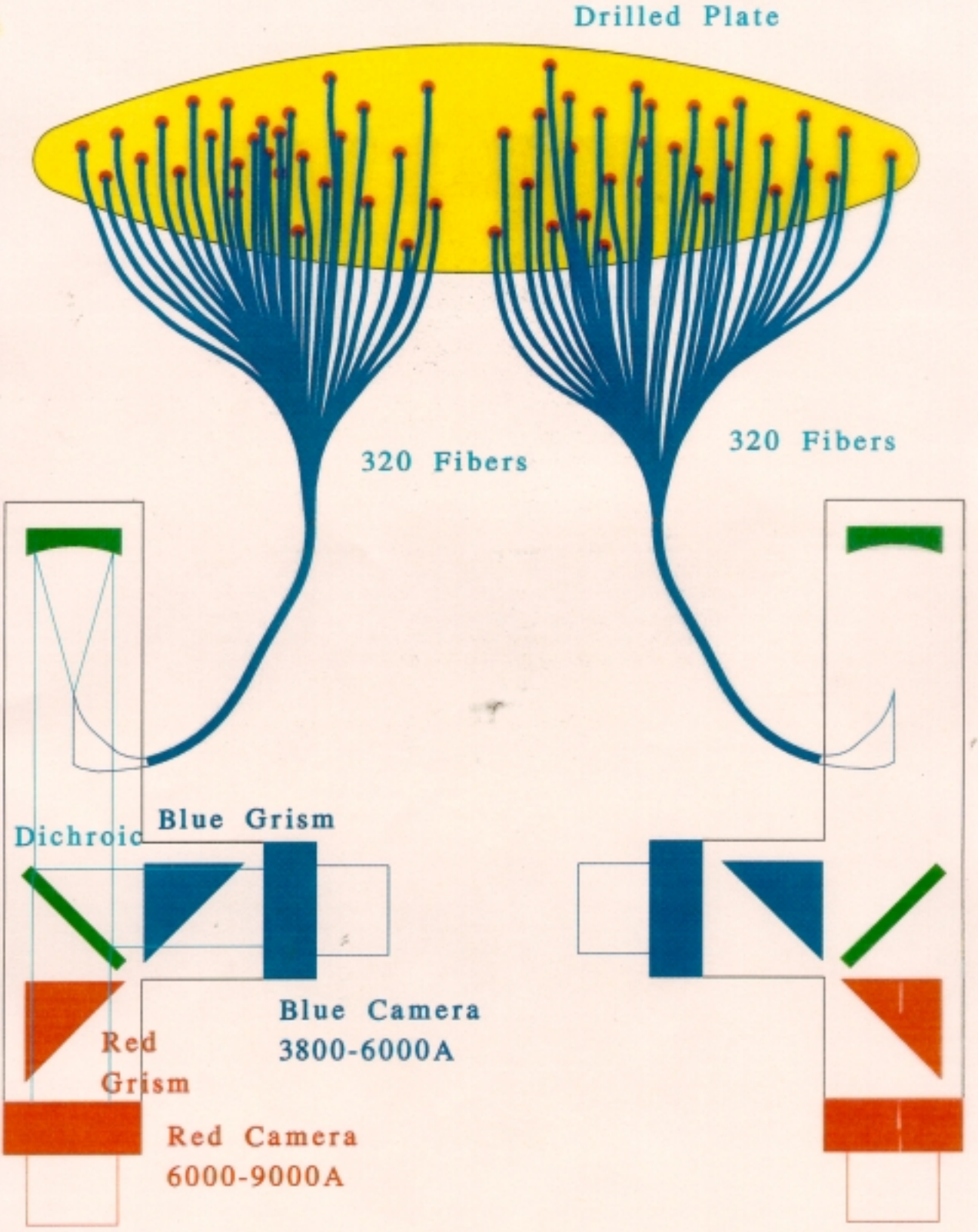

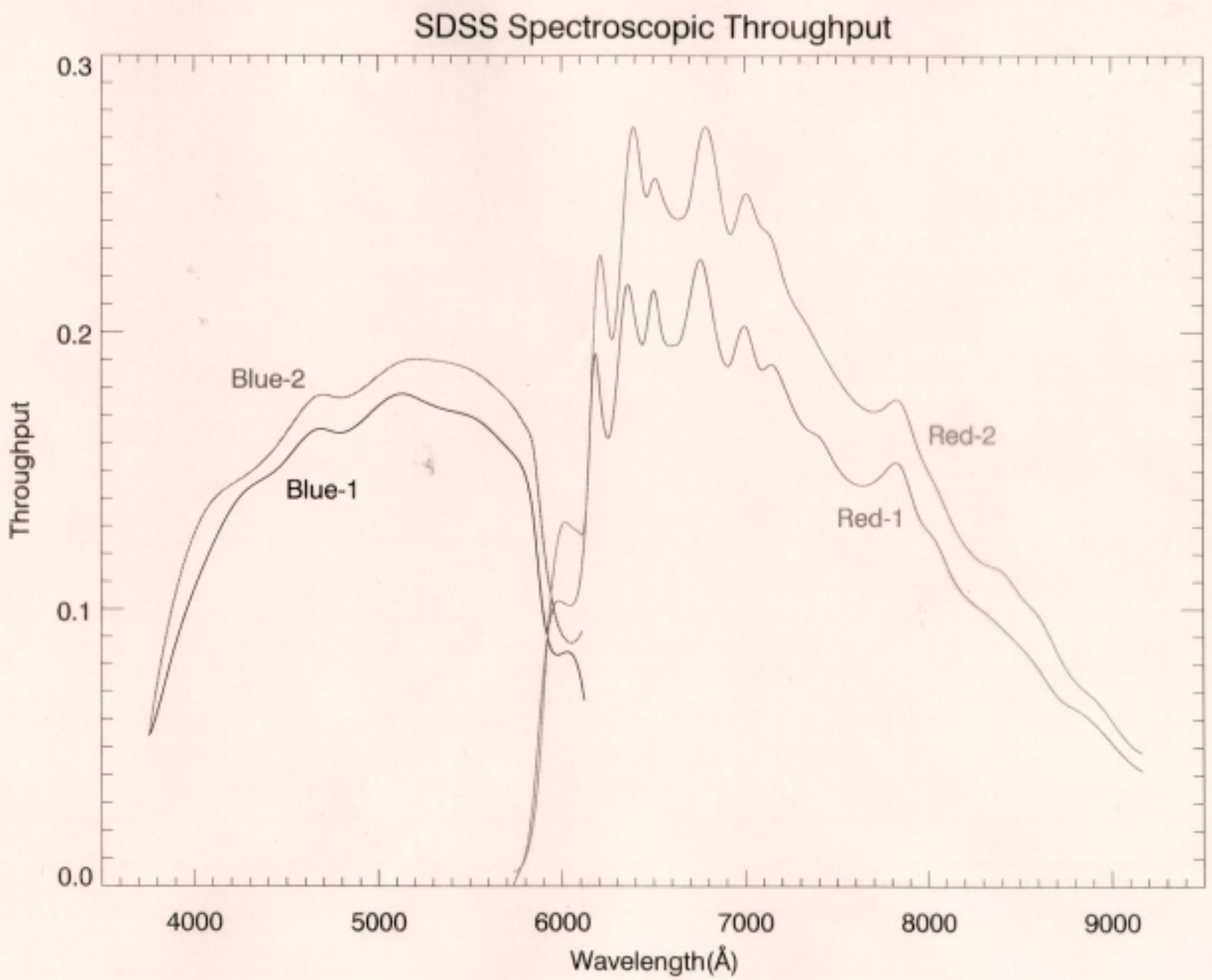
SDSS Spectroscopic Throughput
Throughput
0.3
0.2
0.1
0.0
Blue-2
Blue-1
Red-2
Red-1
4000
5000
6000
7000
8000
9000
Wavelength(Å)

SDSS Operations

- Obtain imaging scans of stripes on the sky.
- Photometric Telescope determines atmospheric extinction coefficients.
- Photometric Telescope also determines photometric zeropoints in calibration patches.
- Determine astrometric solution via grid of Tycho/Hipparcos stars.
- Reduce imaging data to corrected frames, and object catalogs.
- Select Spectroscopic targets according to uniform criteria.
- Assign targets to spectroscopic plates to maximize observing efficiency.
- Drill spectroscopic plates.
- Hand-plug plates, and determine correspondence between fiber number and object number using the plate mapper.
- Observe plate spectroscopically.

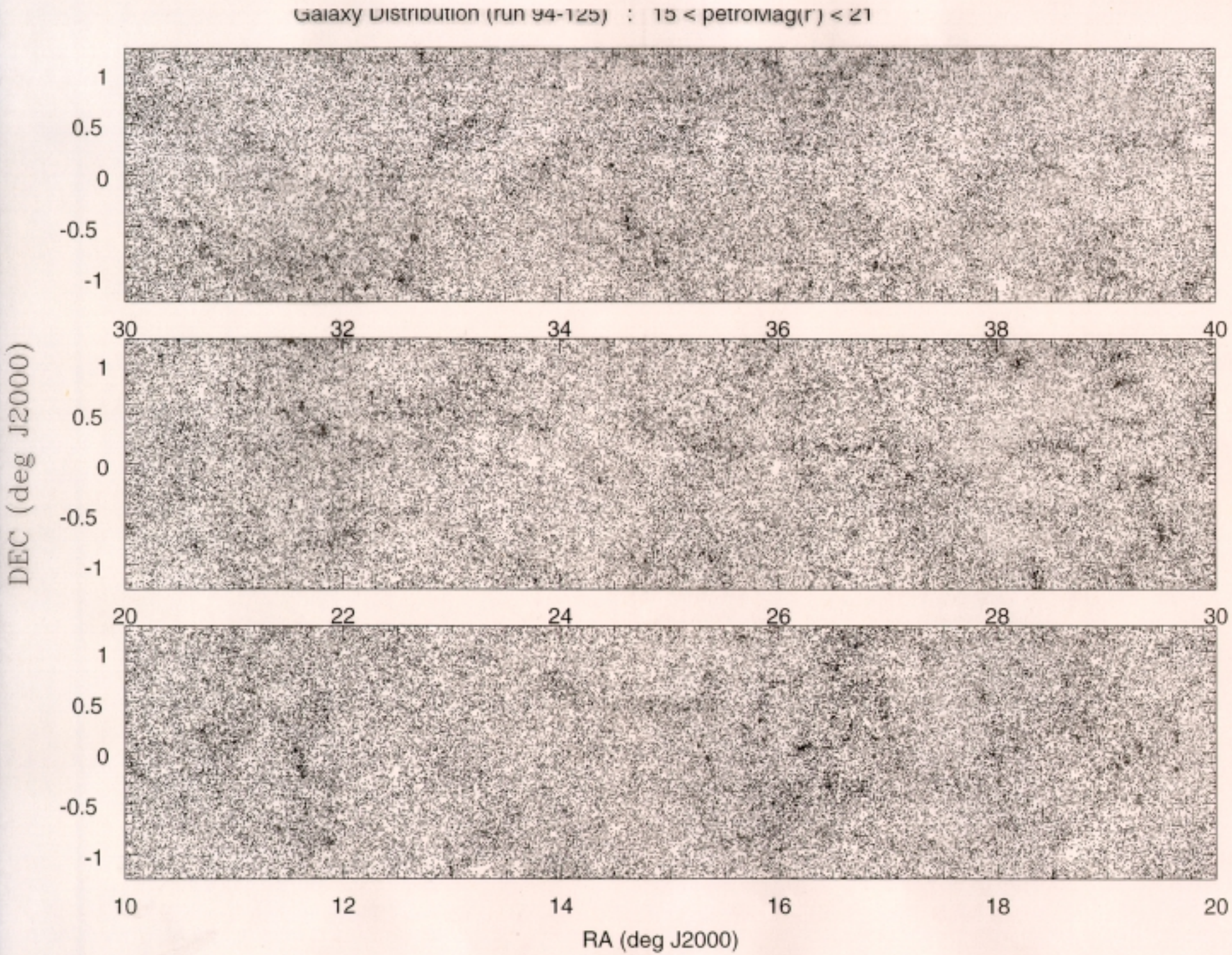
Galaxy Distribution (run 94-125) : 15 < petroMag(r') < 21
DEC (deg J2000)
RA (deg J2000)
1
0.5
0
-0.5
-1
30
32
34
36
38
40
20
22
24
26
28
30
10
12
14
16
18
20

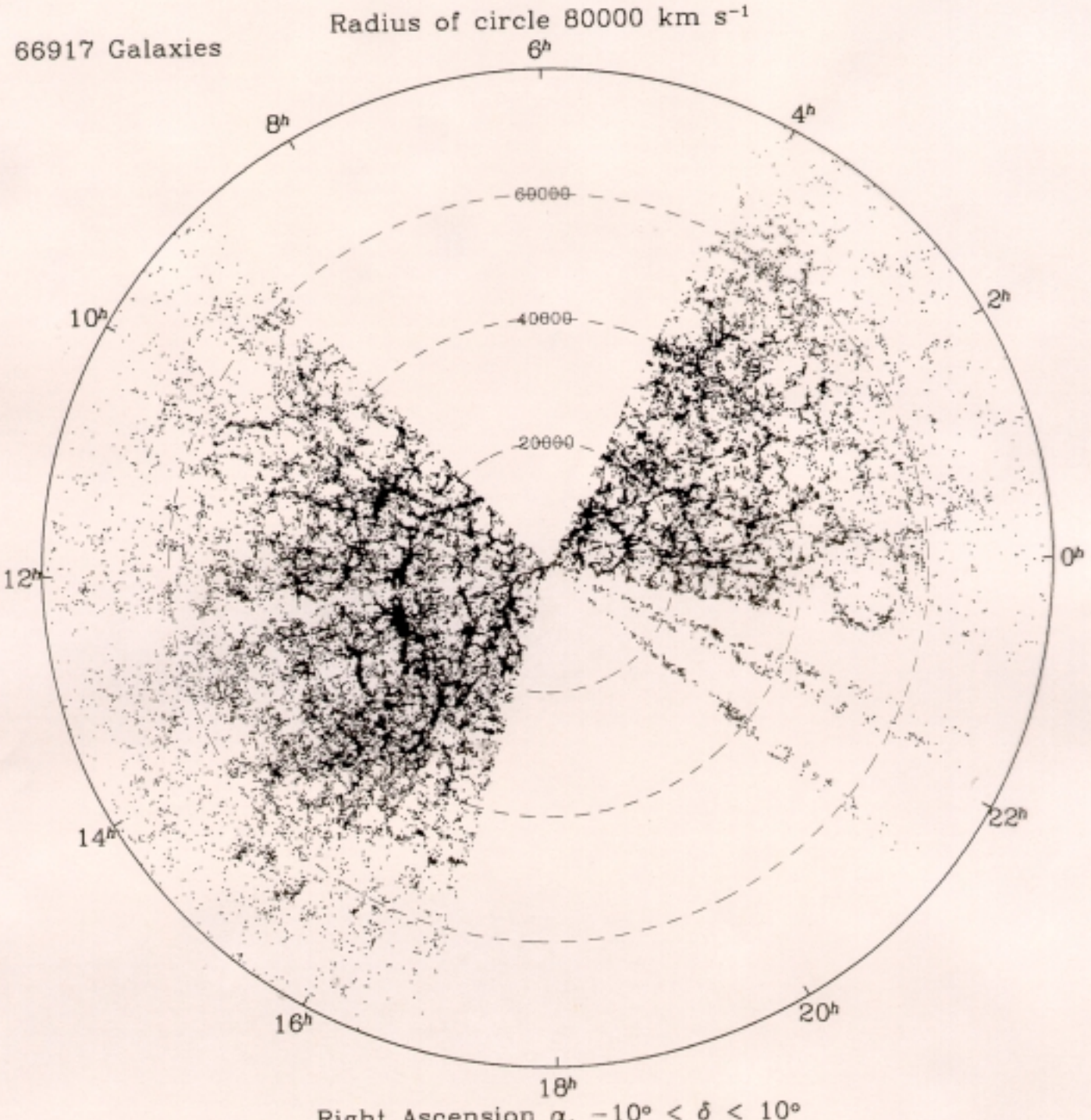
66917 Galaxies
Radius of circle 80000 km s^{-1}
6^h
4^h
2^h
0^h
22^h
20^h
18^h
16^h
14^h
12^h
10^h
8^h
60000
40000
20000
Right Ascension α, −10° < δ < 10°

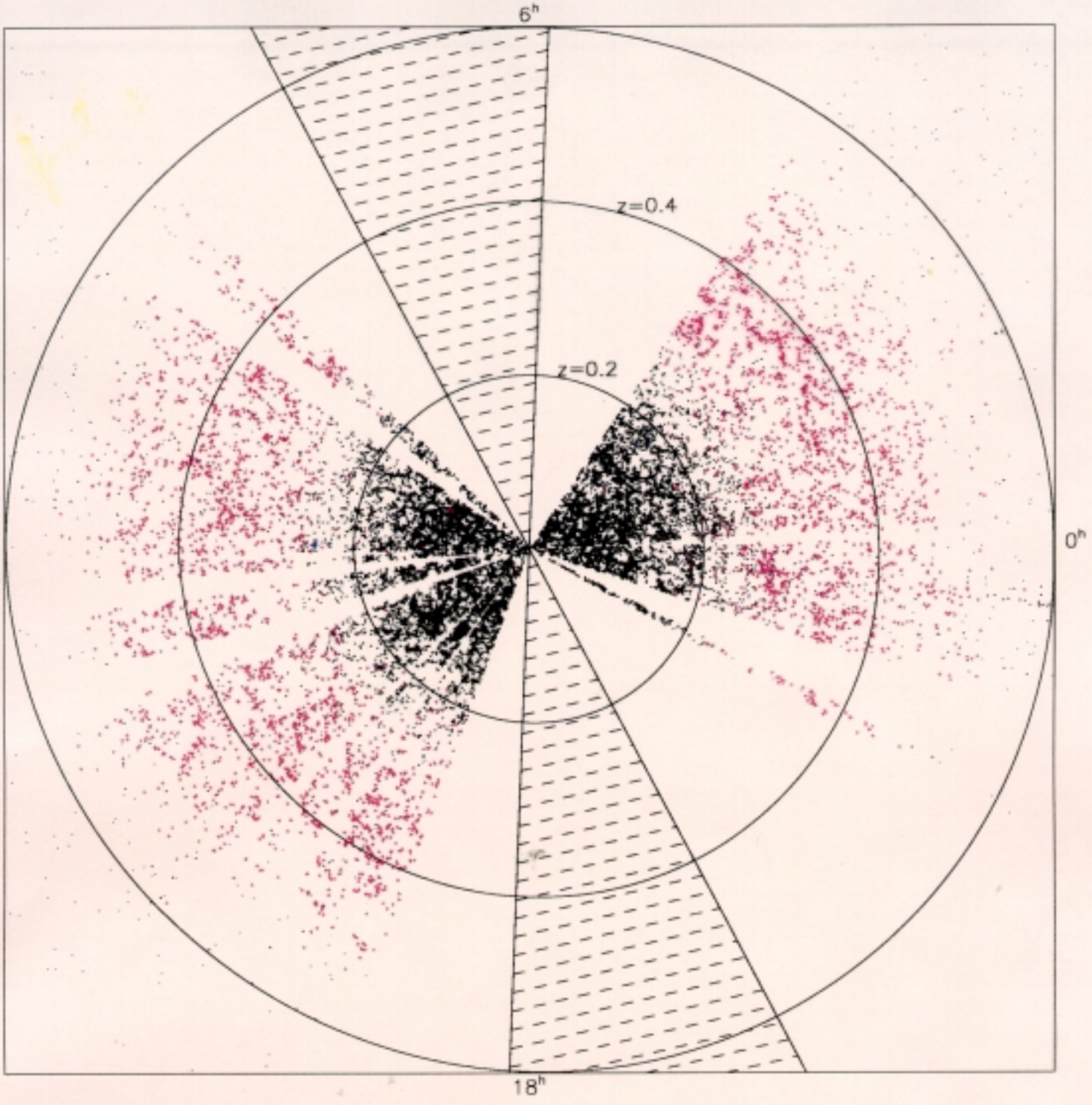
6h
z=0.4
z=0.2
0h
18h

θ_μ
0_μ
18_μ
z=4
z=3
z=2
z=1

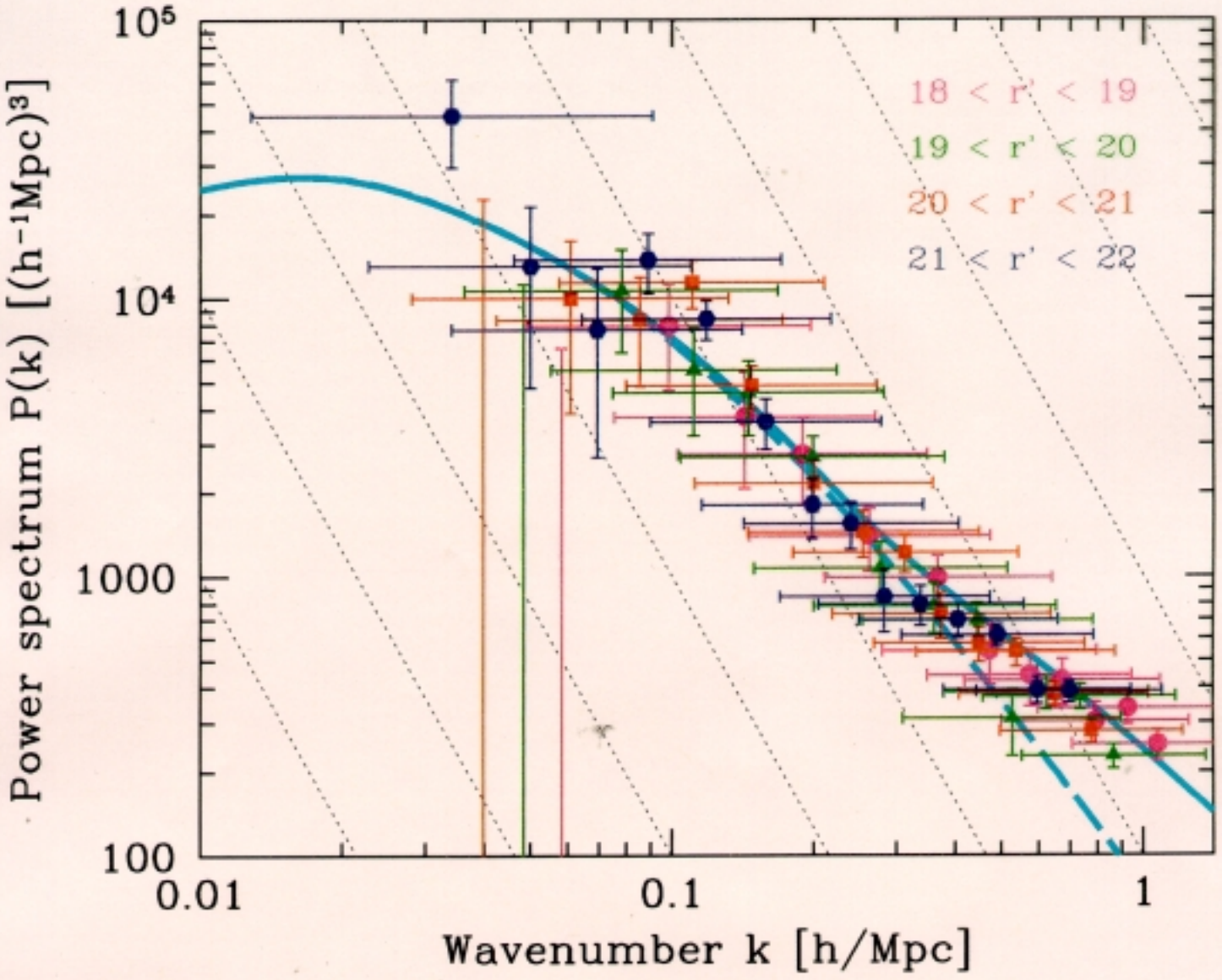
Power spectrum P(k) [(h⁻¹Mpc)³]
10⁵
10⁴
1000
100
0.01
0.1
1
Wavenumber k [h/Mpc]
18 < r' < 19
19 < r' < 20
20 < r' < 21
21 < r' < 22

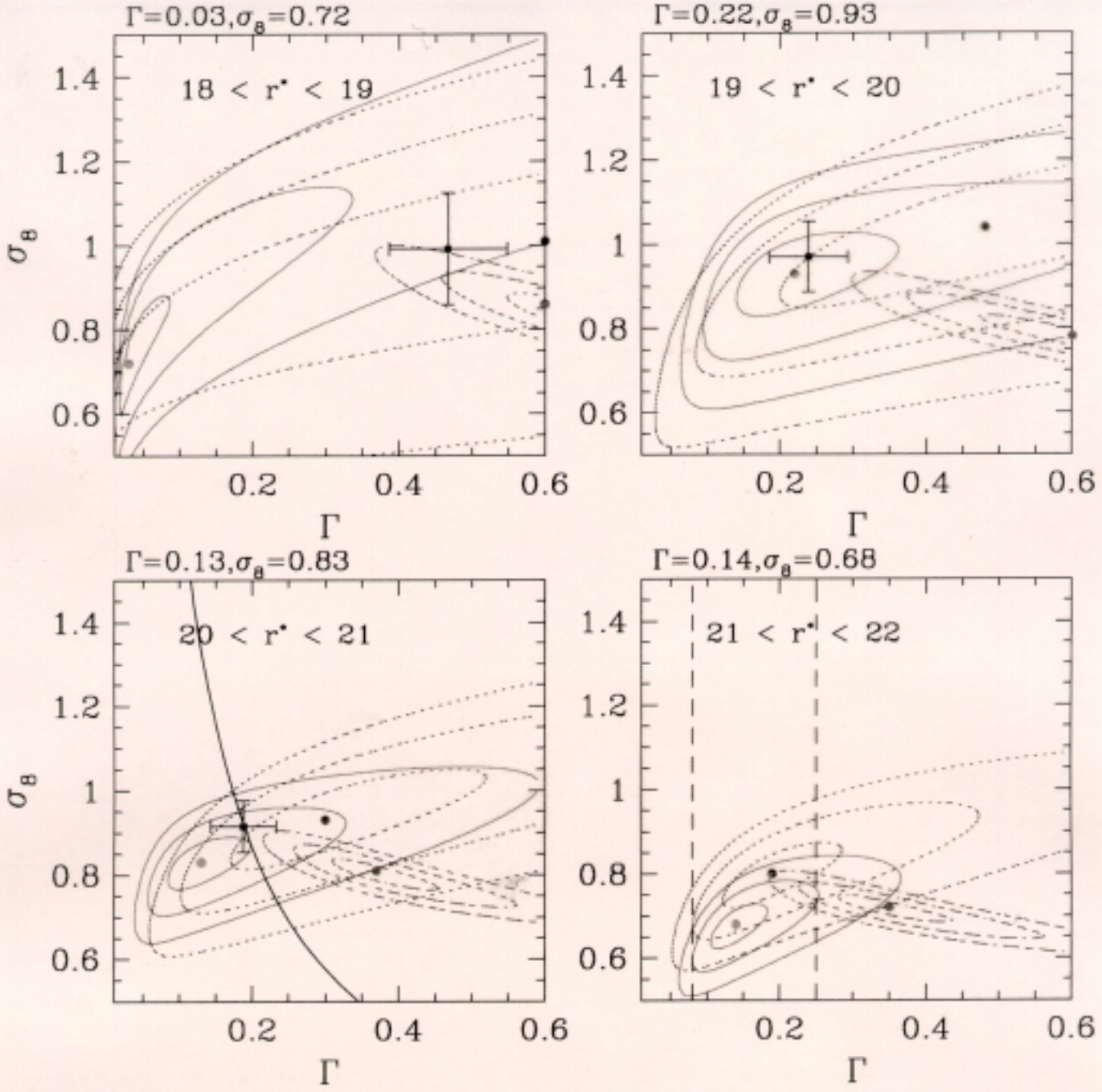
Γ=0.03,σ8=0.72
18 < r* < 19
Γ=0.22,σ8=0.93
19 < r* < 20
Γ=0.13,σ8=0.83
20 < r* < 21
Γ=0.14,σ8=0.68
21 < r* < 22
σ8
Γ
0.6
0.8
1
1.2
1.4
0.2
0.4
0.6

(Richards, Fan, Newberg, Schneider et al...)

Selection of Quasars

- Ordinary stars fall along a one-dimensional locus in color-color space, depending on surface temperature.
- Low redshift quasars are blue; colors are insensitive to redshift. Distinguished from hot stars by the lack of a Balmer jump.
- As the Lyman α forest is redshifted into the filters, a quasar's colors become red.
- Quasars with $z > 3.5$ are reddened in $g - r$.
- Quasars with $z > 4.5$ are reddened in $r - i$.
- Quasars with $z > 5.3$ are reddened in $i - z$.

Selection of outliers in parameter space is quite straightforward. A quasar candidate is defined as any object far from the stellar locus. This works because the data are **clean** and **precise**; unreliable photometry is properly flagged as such.

But see Bob Nichol's talk for another approach using mixture model.

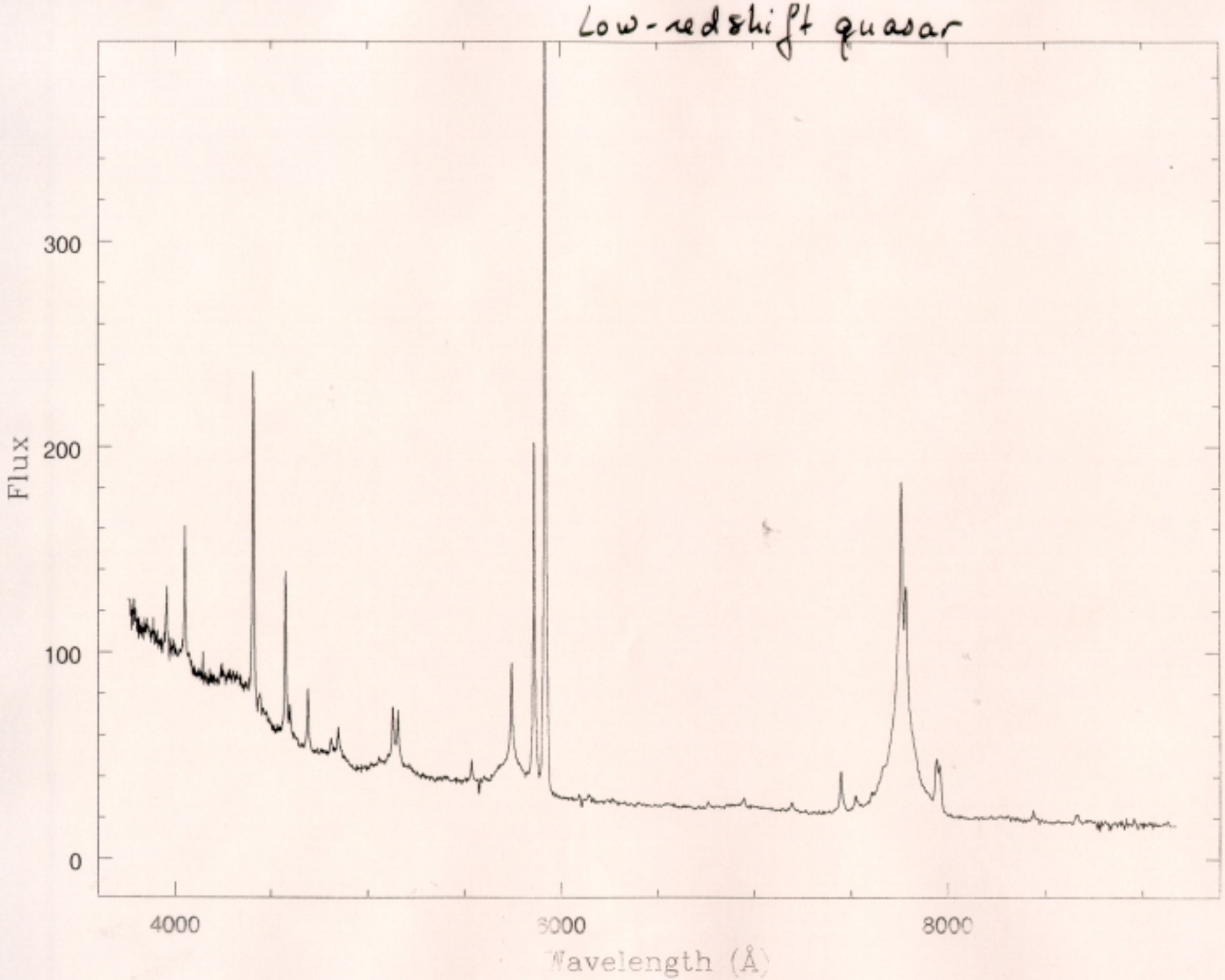
Low-redshift quasar
300
200
100
0
Flux
4000
8000
Wavelength (Å)

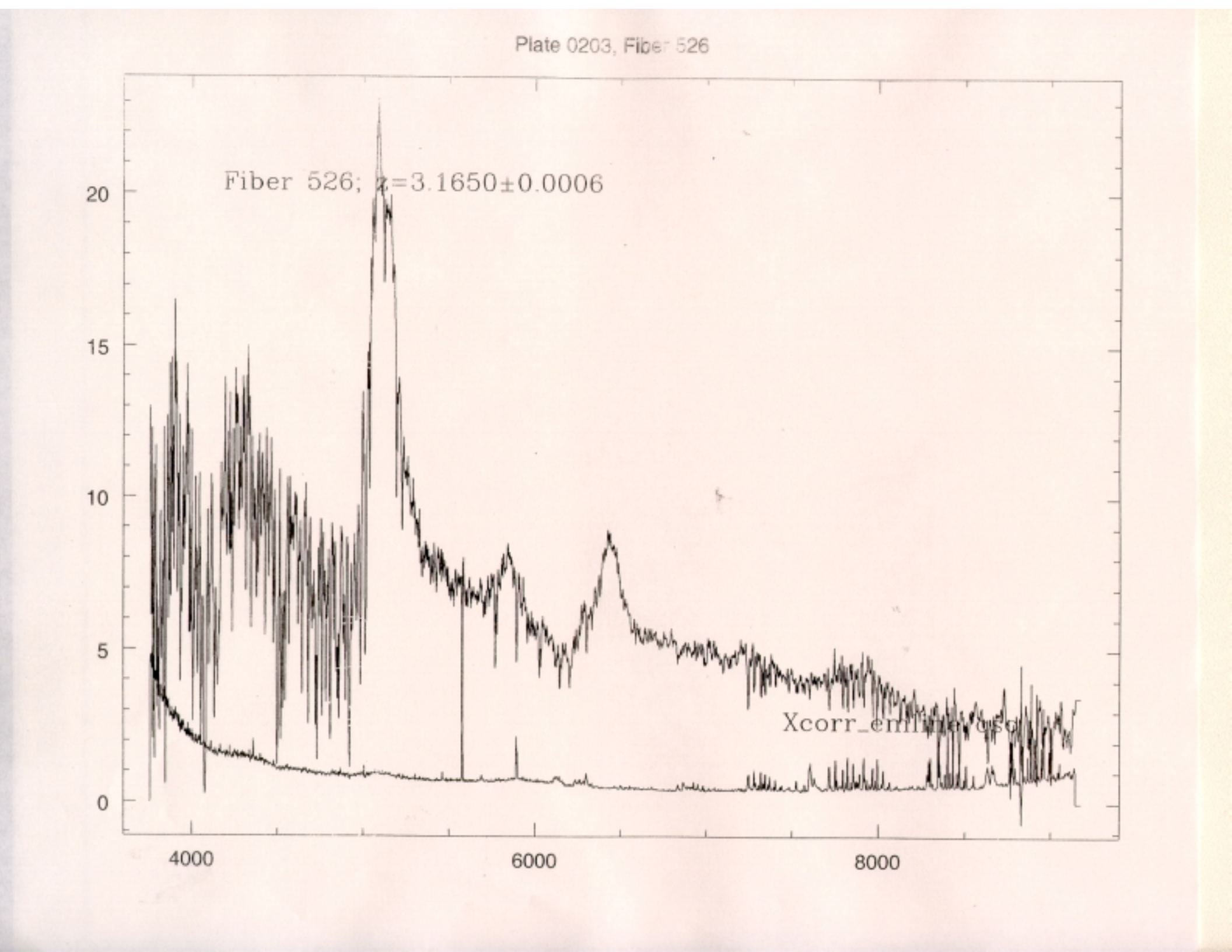
Plate 0203, Fiber 526
Fiber 526; z=3.1650±0.0006
20
15
10
5
0
4000
6000
8000

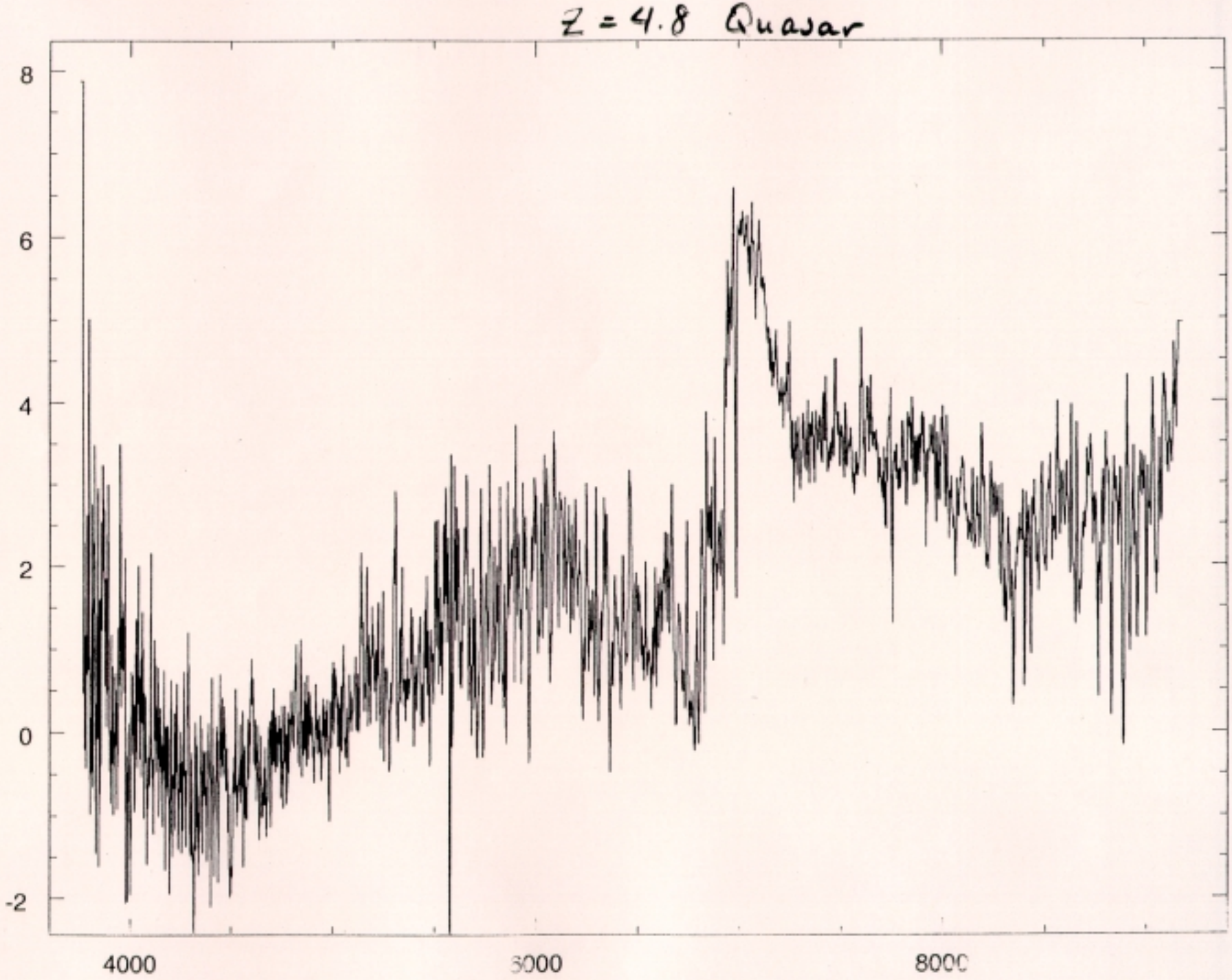
z = 4.8 Quasar
8
6
4
2
0
-2
4000
6000
8000

25 square degrees to $i' = 21$

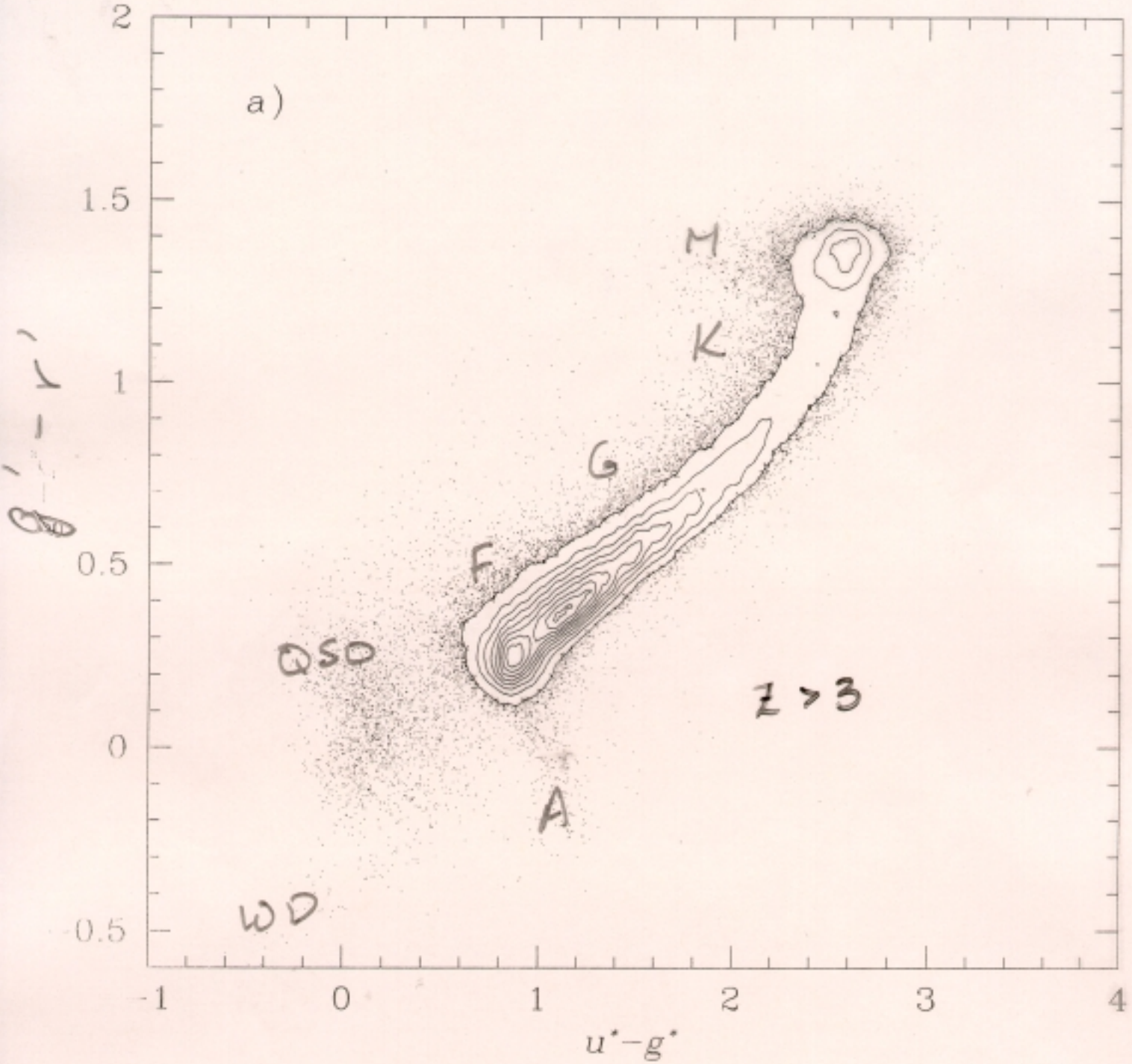

$u'-g'$

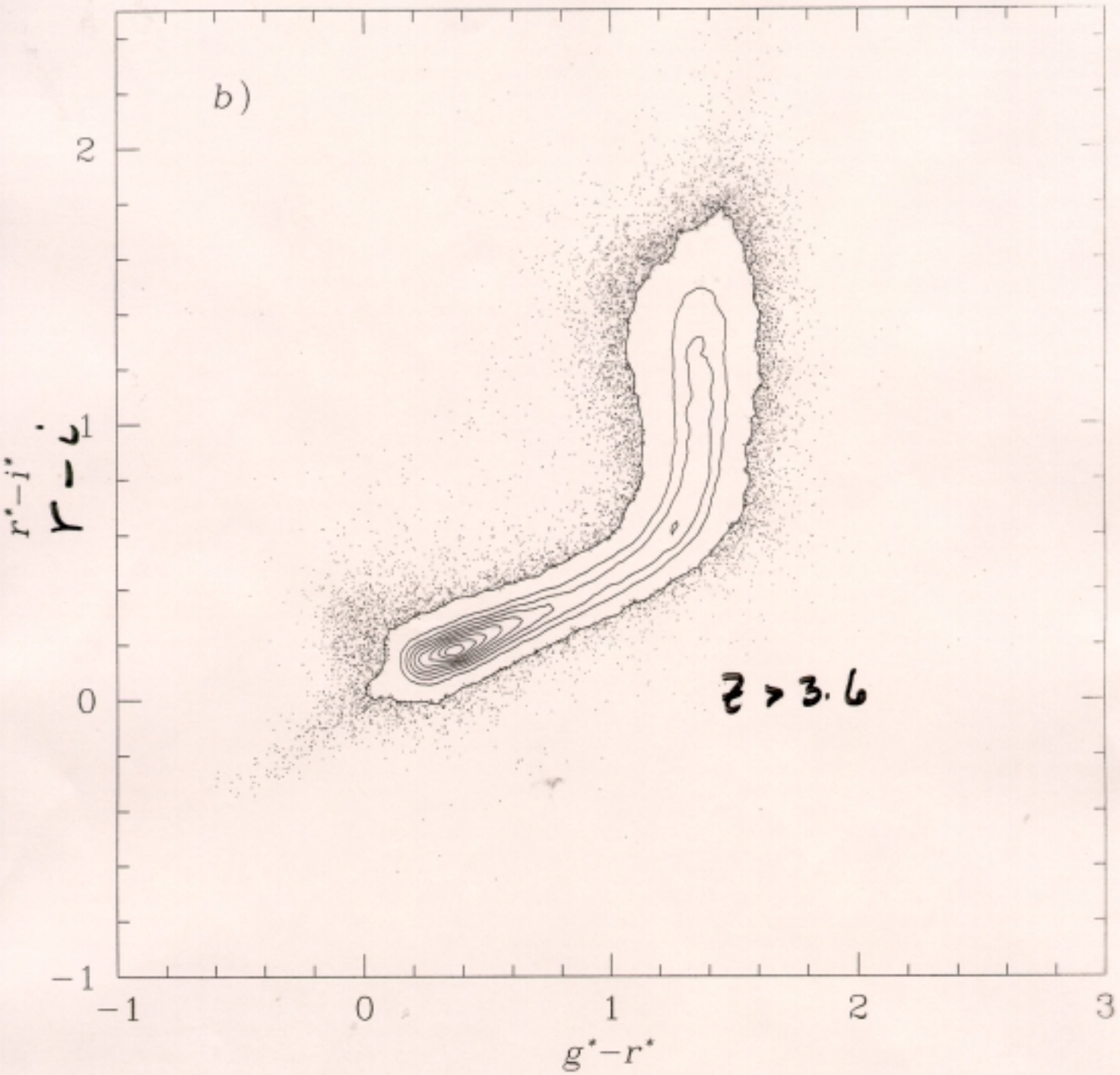
b)
z > 3.6
r'−i'
g'−r'
2
1
0
−1
−1
0
1
2
3

- The quasar number density drops by a factor of 6 from $z = 3.5$ to $z = 5.0$.
- Luminosity function slope is *shallower* than at low-z; inconsistent with pure density or luminosity evolution.
- $z = 5$ quasar is detected at 1.2mm; dust mass of $10^8\,M_\odot$.
- Discovery of a $z = 4.62$ quasar *without emission lines*; several other examples exist.
- Metal emission lines are present at high redshift.
- The $z = 5.8$ quasars are *luminous*, $M_B = -27.5$.
- The first $z = 5.8$ quasar is a BAL quasar; underluminous in X-rays.
- Close pairs of quasars exist at high redshift.

Evolution of Quasar number Density.

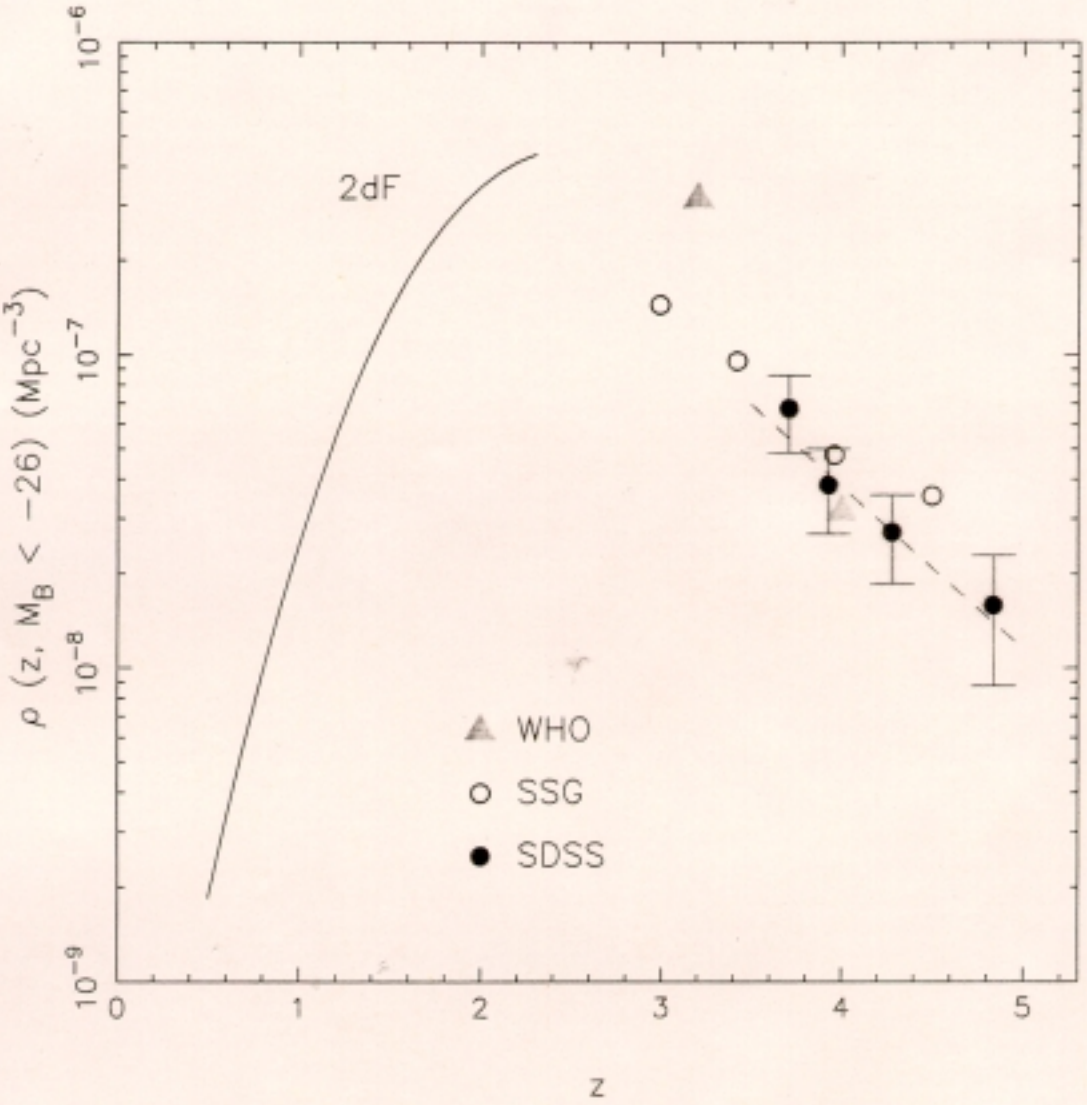

Figure 3. The evolution of the quasar spatial density at $M_B < -26$ is compared with previous studies. The SDSS points shown are the results using the C^- estimator, and the dashed line is the maximum likelihood solution. The SSG points shown are the spatial density calculated with the $1/V_a$ method. The low-redshift result is the best-fit model from the 2dF survey (Boyle et al. 2000).

High−z Quasar Pairs in Equatorial Stripe

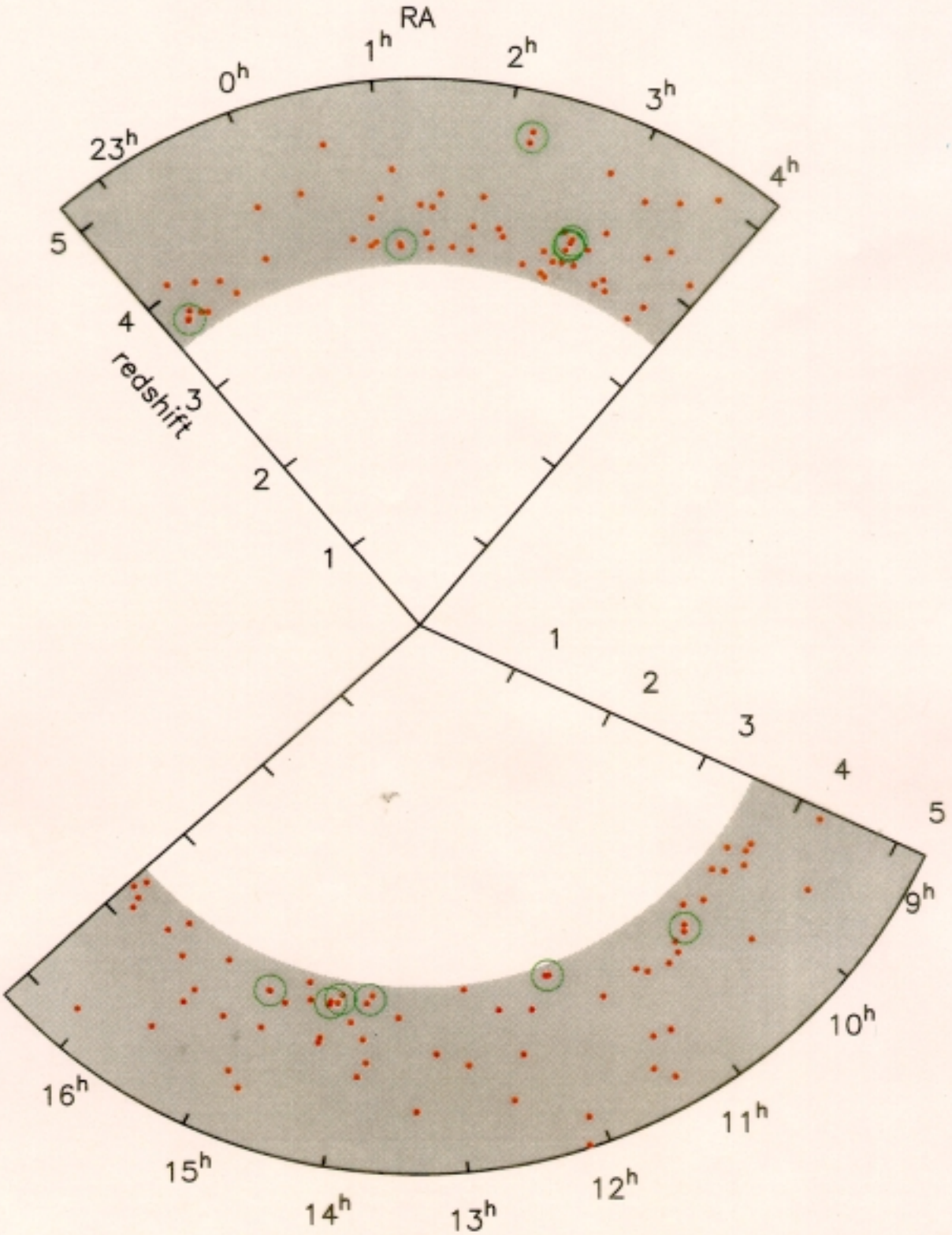

Our approach has been:

- Recognize cosmic rays by their sharp gradients relative to the point spread function; follow this selection up by eyeball inspection.
- Carry out repeat z band photometry to reject further cosmic rays, and to recognize when the photometry is biased.
- Carry out J-band photometry (11,000Å) to distinguish cool stars from quasars.

This works! Only four objects remain with our cuts on $i - z$ and $z - J$; **all** are high-redshift quasars.

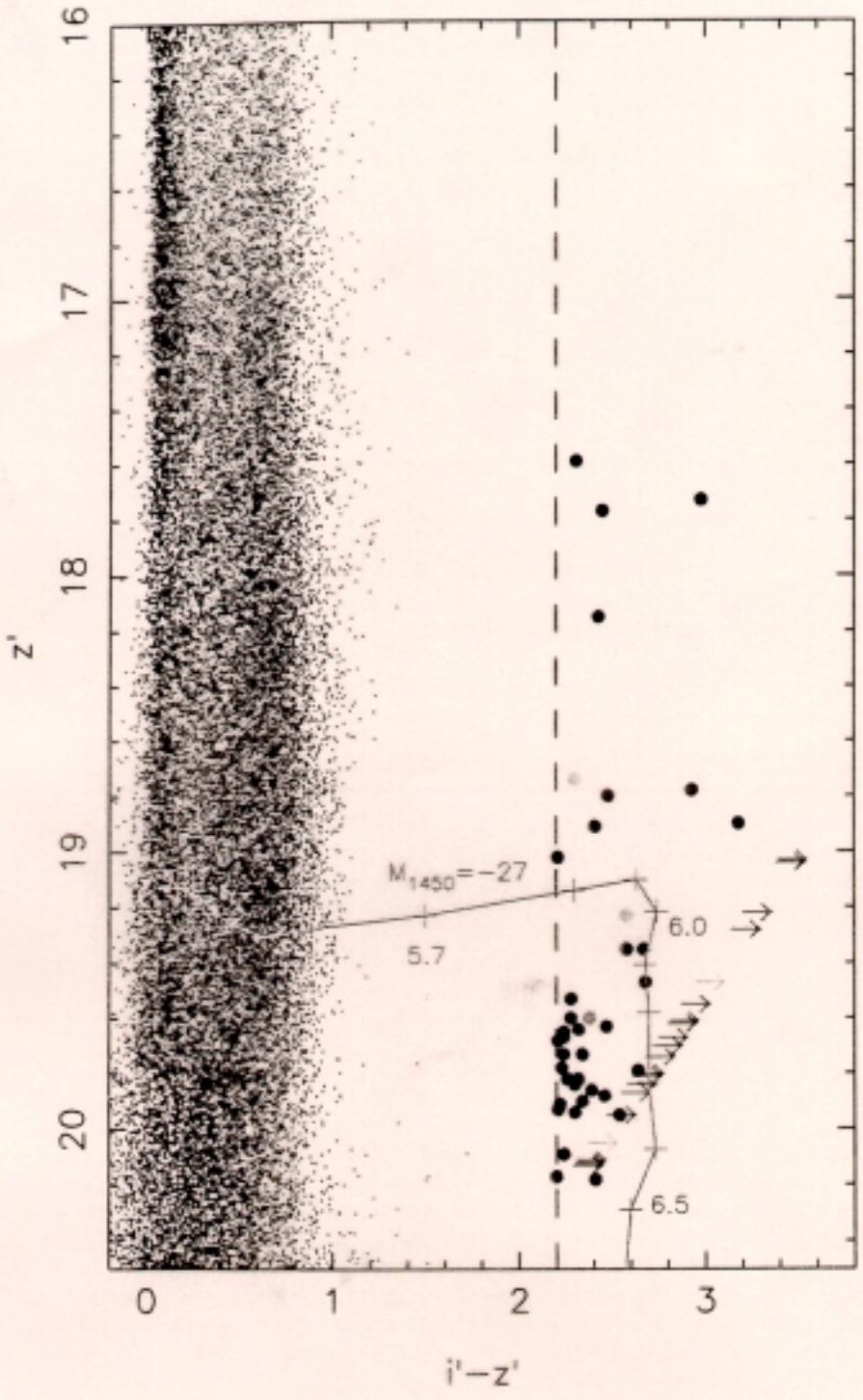

Figure 1. $i' - z'$ vs. z' color-magnitude diagram, I want to add a track of $M_B = -27$ quasars. Need to decide use luptitude or upper limit.

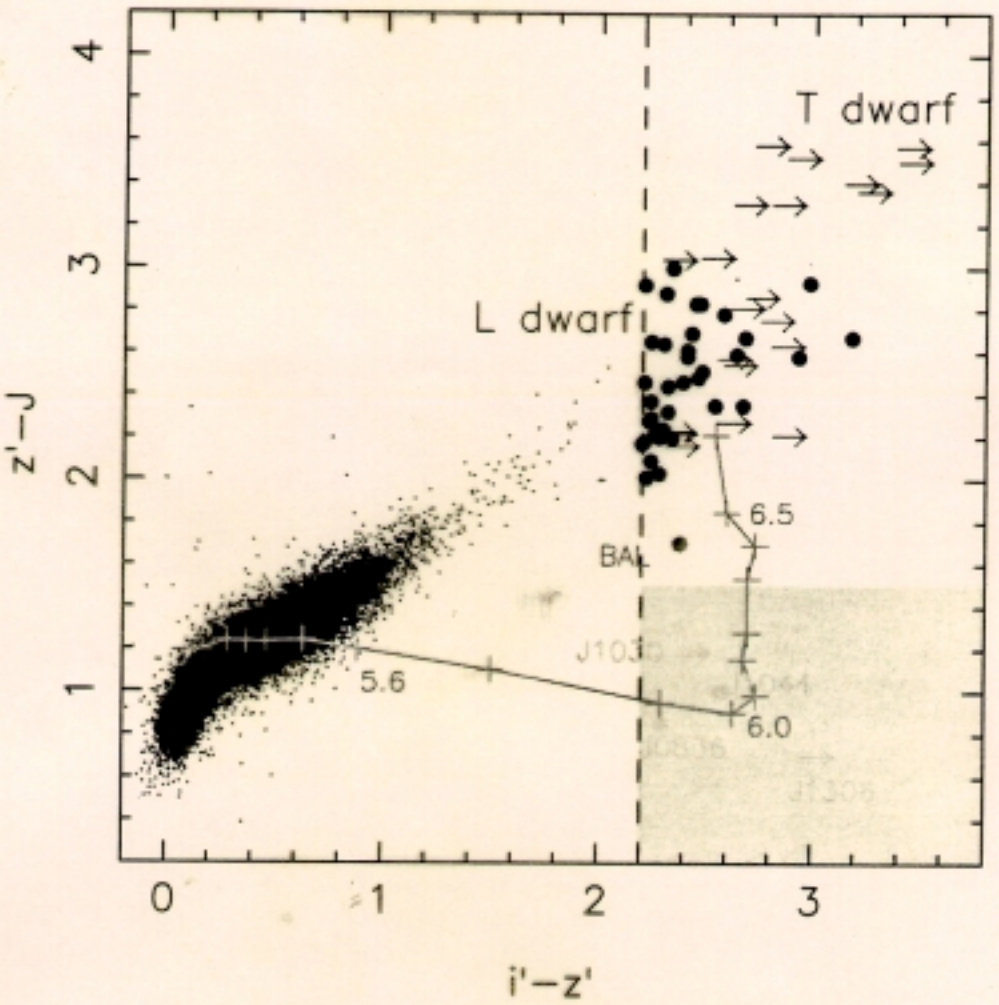

Figure 2. $i' - z'$ vs. $z' - J$ color-color diagram

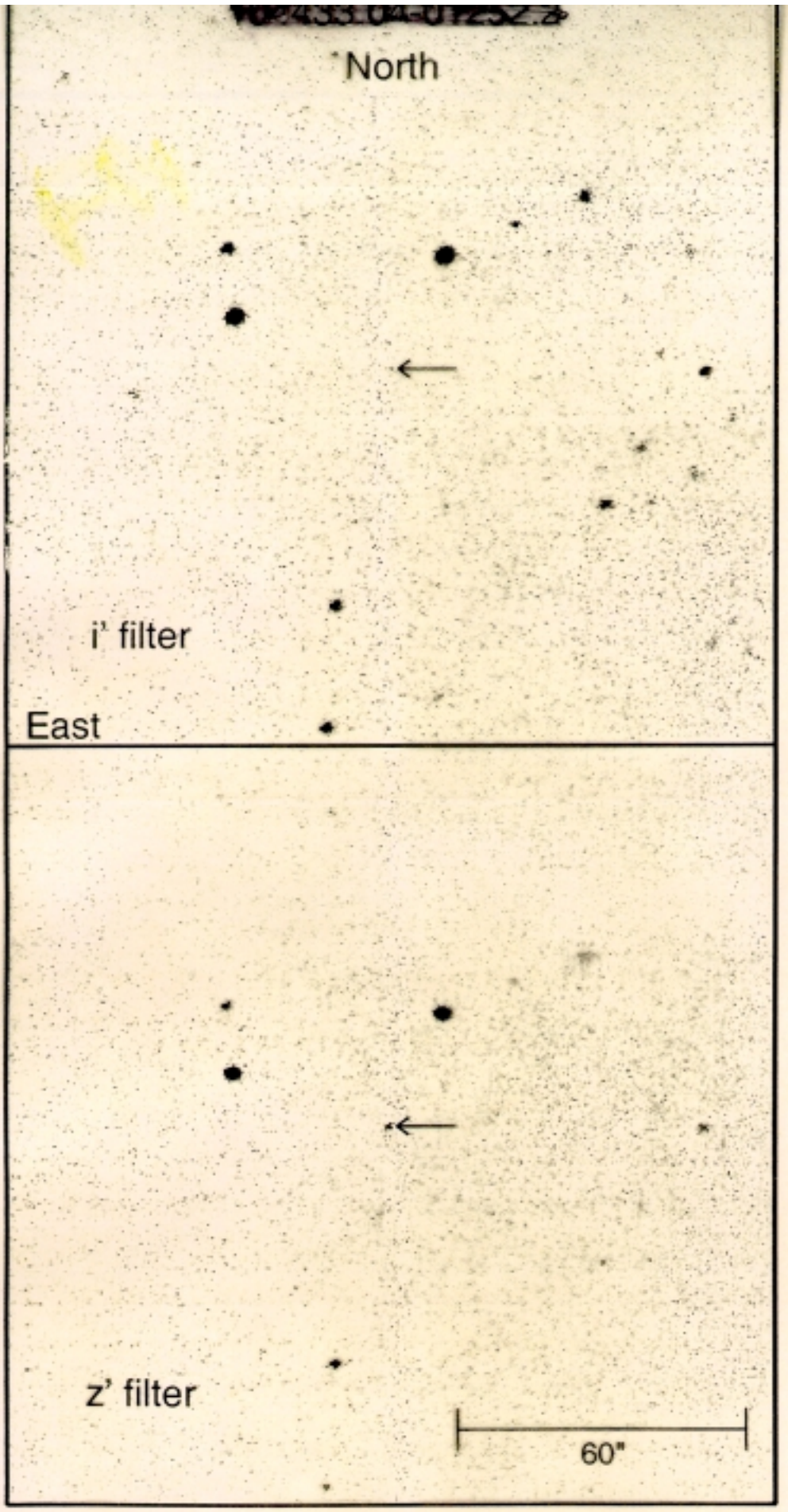

$i' - z' = 2.6$

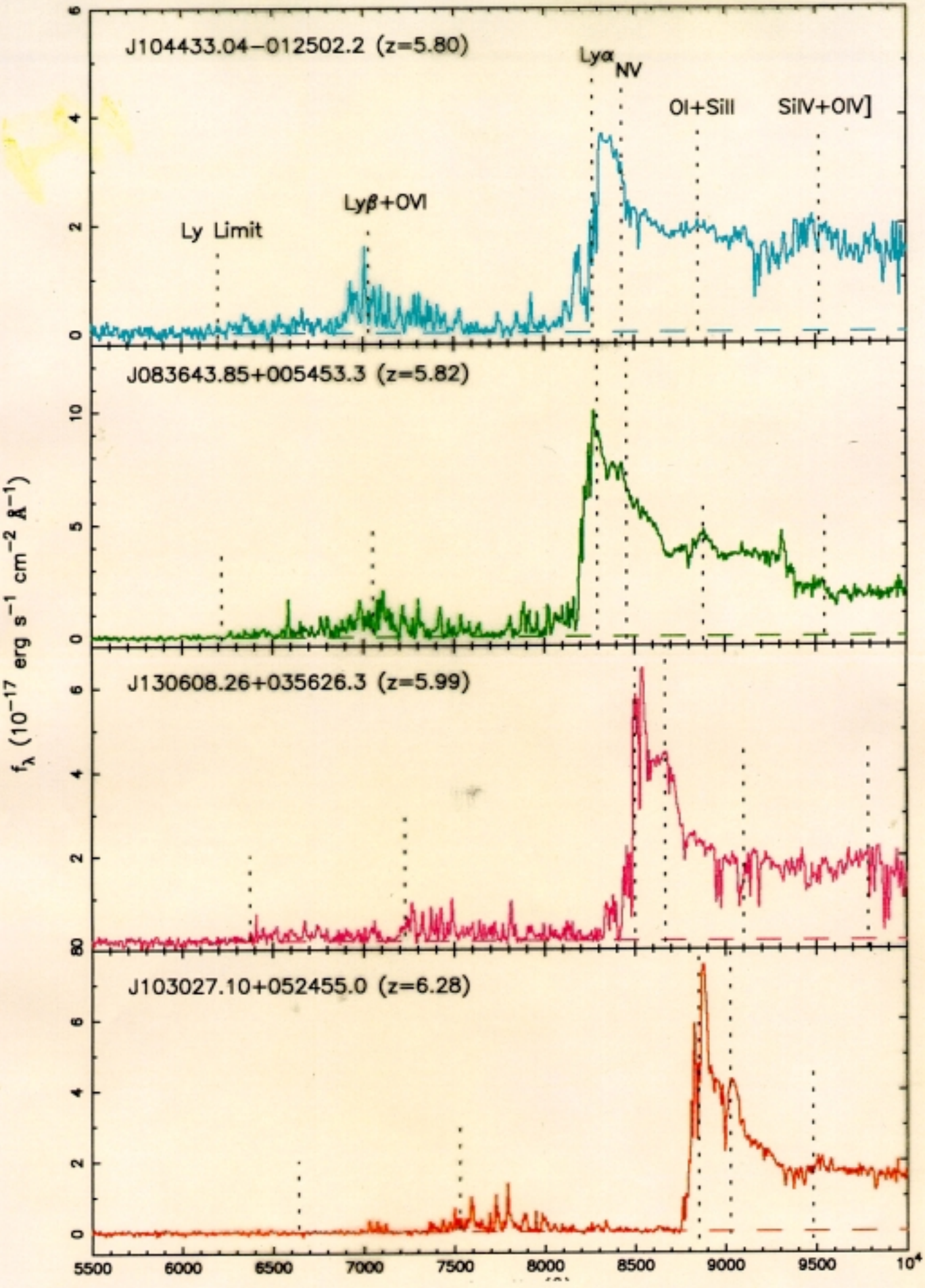
J104433.04−012502.2 (z=5.80)
Lyα
NV
OI+SiII
SiIV+OIV]
Lyβ+OVI
Ly Limit
J083643.85+005453.3 (z=5.82)
J130608.26+035626.3 (z=5.99)
J103027.10+052455.0 (z=6.28)
f_λ (10^{-17} erg s^{-1} cm^{-2} Å^{-1})
5500
6000
6500
7000
7500
8000
8500
9000
9500
10^4

Ly α forest removes 90% of light. Gas between Ly α forest lines still ionized ($\tau < 0.4$)

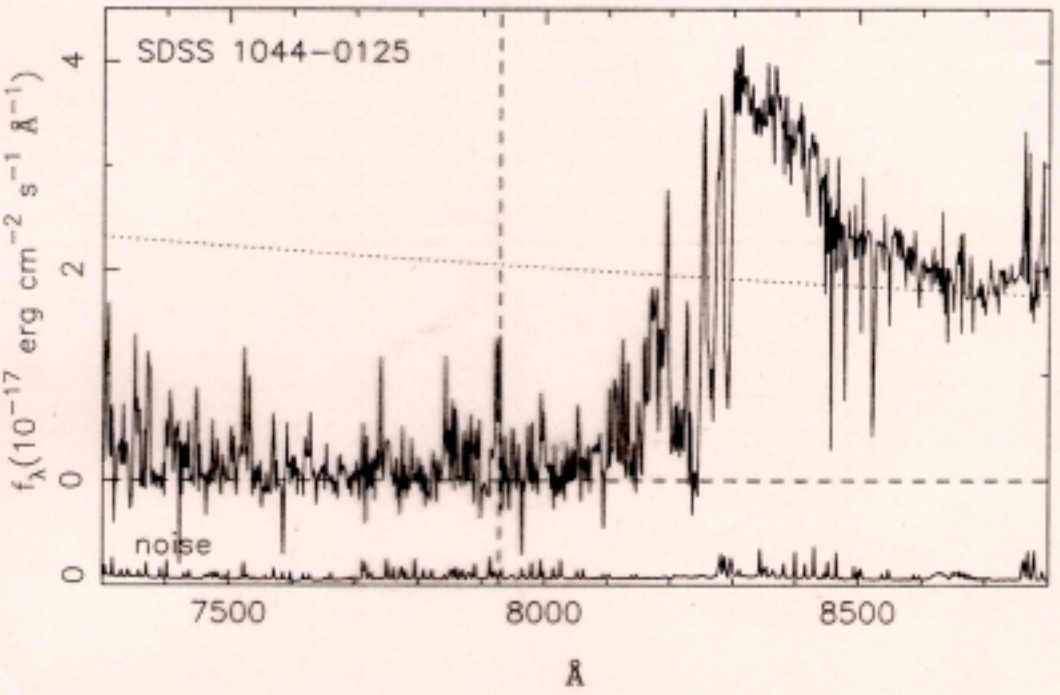

Figure 3. ESI Echellete spectrum over the range 7300 – 8800 Å. The spectrum has been smoothed to a resolution of 2 Å. The dotted line shows a $\nu^{-0.5}$ continuum fit, normalized to the region 8500 – 8600 Å. The dashed line indicates the region with minimum opacity ($\tau \sim 0.4$, see §3.1).

The Gunn-Peterson Effect: First Light in the Universe

Neutral hydrogen has a large cross-section for Lyα line absorption. Distributed over a range of redshifts, this would cause an absorption trough in the spectrum of quasars. Thus the presence of detected flux in quasars blueward of the Lyα emission line indicates that hydrogen gas is not neutral. Small pockets of neutral hydrogen do exist, and give rise to the *Lyman α forest.*

This gas is ionized by ultraviolet photons from quasars, and from hot stars in galaxies.

At early enough times, there was presumably not enough quasars and stars formed yet, thus the gas should be neutral.

We have now seen the signature of this effect; the hydrogen absorption trough is seen in the spectrum of the highest redshift quasar known. This corresponds to a time $\approx 10^9$ years after the Big Bang.

We put a lower limit of $\tau = 5.5$ on the optical depth. Purely neutral hydrogen would give $\tau = 10^5$. Measuring the difference between $\exp[-5.5]$ and $\exp[-10^5]$ is not easy!

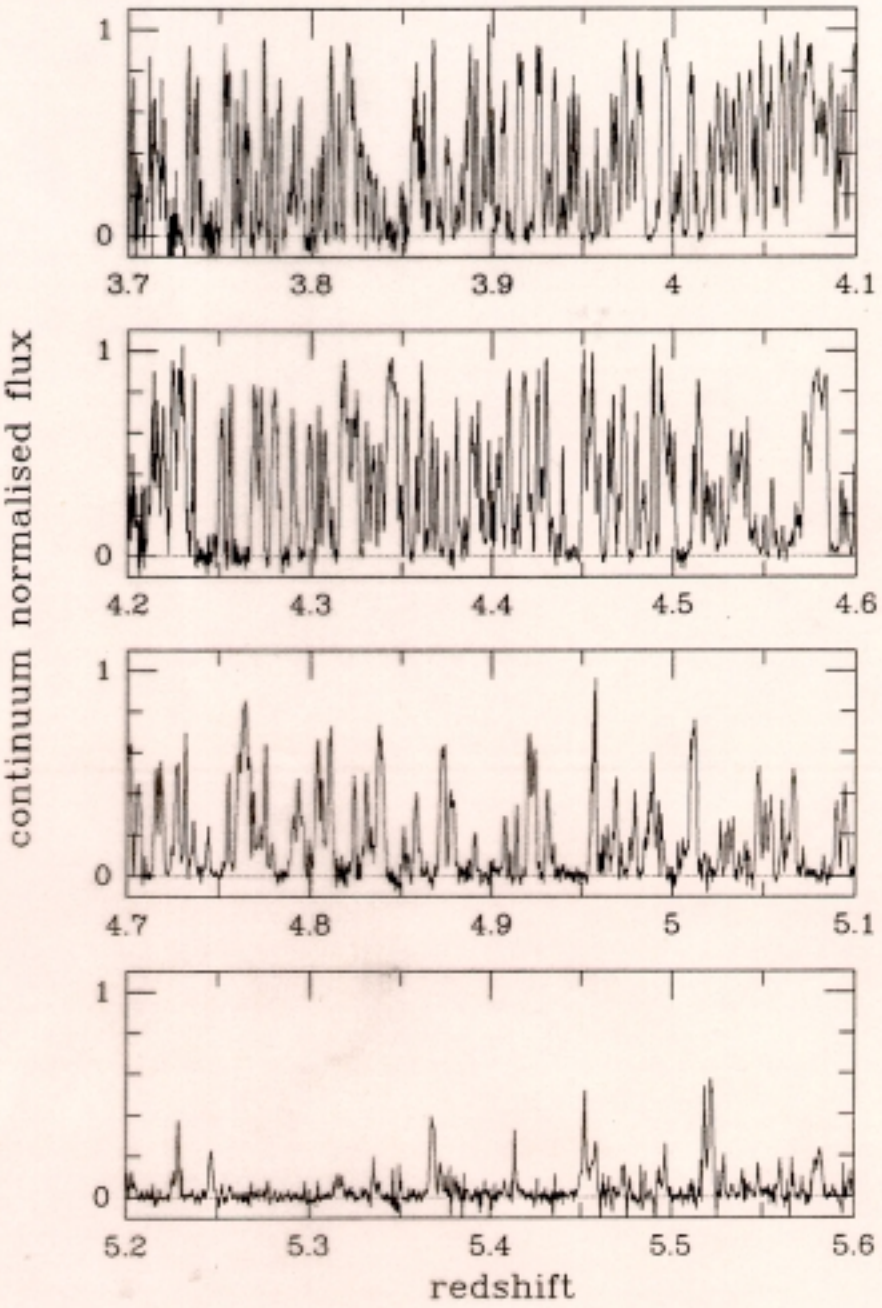

Fig. 3.— A schematic illustration of the evolution of the Lyα forest, in four redshift intervals. The top two windows are from a spectrum of SDSS 1737+5828 at $z = 4.94$, observed with the same instrument; the bottom two are from the spectum of SDSS 1044–0125, presented here. The spectra have been renormalised by the best estimate of the continuum (for the bottom two panels, we used the middle power-law shown in Fig. 1).

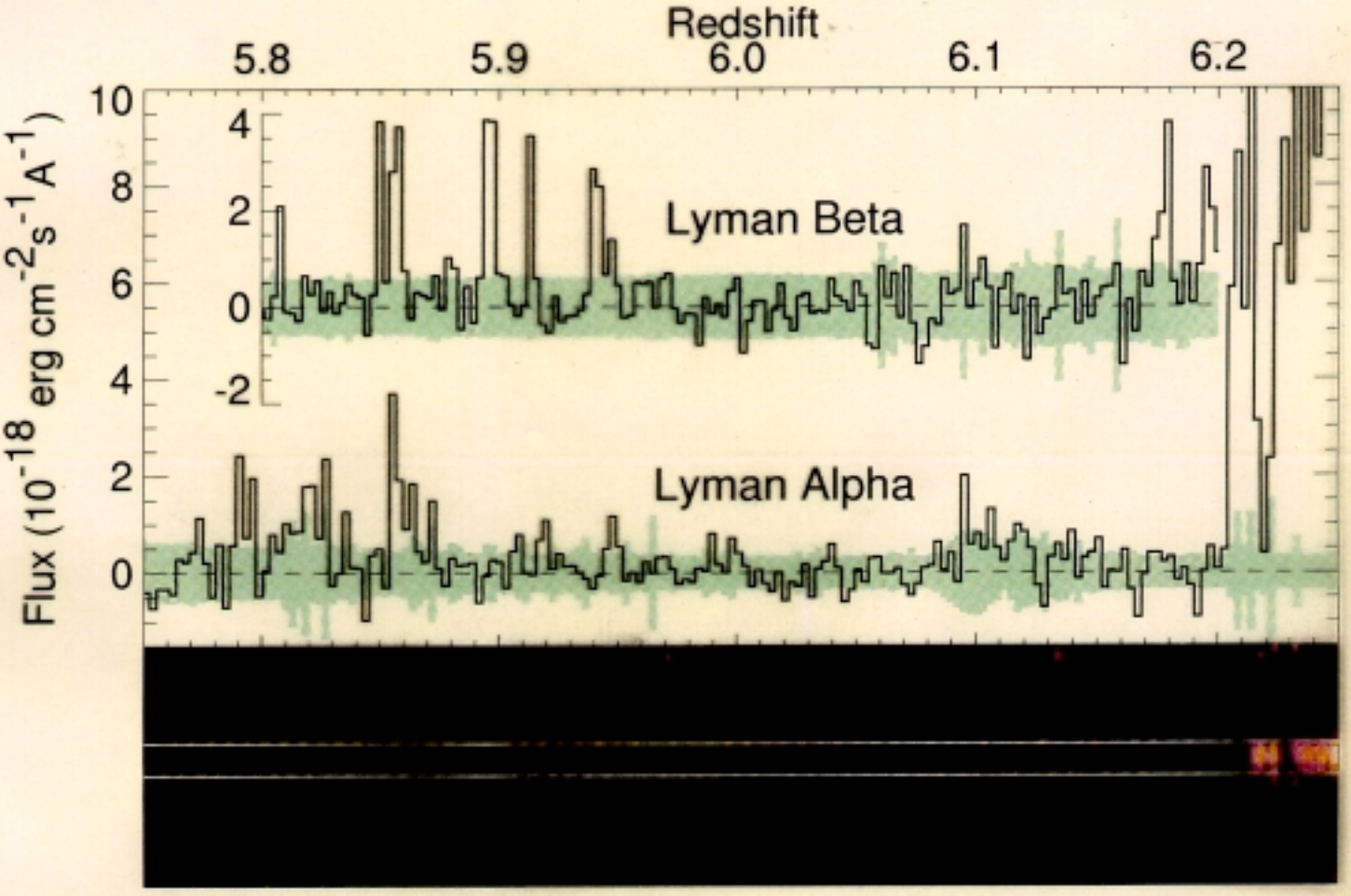
Redshift
5.8
5.9
6.0
6.1
6.2
Flux (10^{-18} erg cm^{-2}s^{-1}A^{-1})
10
8
6
4
2
0
4
2
0
-2
Lyman Beta
Lyman Alpha

Discovery of Brown Dwarfs with SDSS

Jill Knapp

M stars have optical spectra dominated by VO and TiO. At $T < 2300$K, these precipitate out of the atmosphere; the spectrum becomes dominated by pressure-broadened lines of alkali metals, and a variety of hydrides.

These *L dwarfs* are extremely red in $i' - z'$, but are relatively blue in $r' - i'$. They are distinct from ordinary stars in the $r' - i', i' - z'$ diagram.

The 2MASS and DENIS surveys have been discovering such objects in large numbers. Presence of Liλ6707 absorption implies that many of these are not burning H in their centers. Thus the relation between temperature and mass depends on age.

SDSS is finding these at roughly the same surface density as 2MASS.

The coolest such object known was Gl 229B, with $T \approx 900$K. Near-infrared spectrum is similar to that of Jupiter; dominated by H_2O and CH_4. SDSS has found several other methane dwarfs in the field, with very similar spectra. Undetected in r', $i' - z' > 3$.

Barrows et al 1997

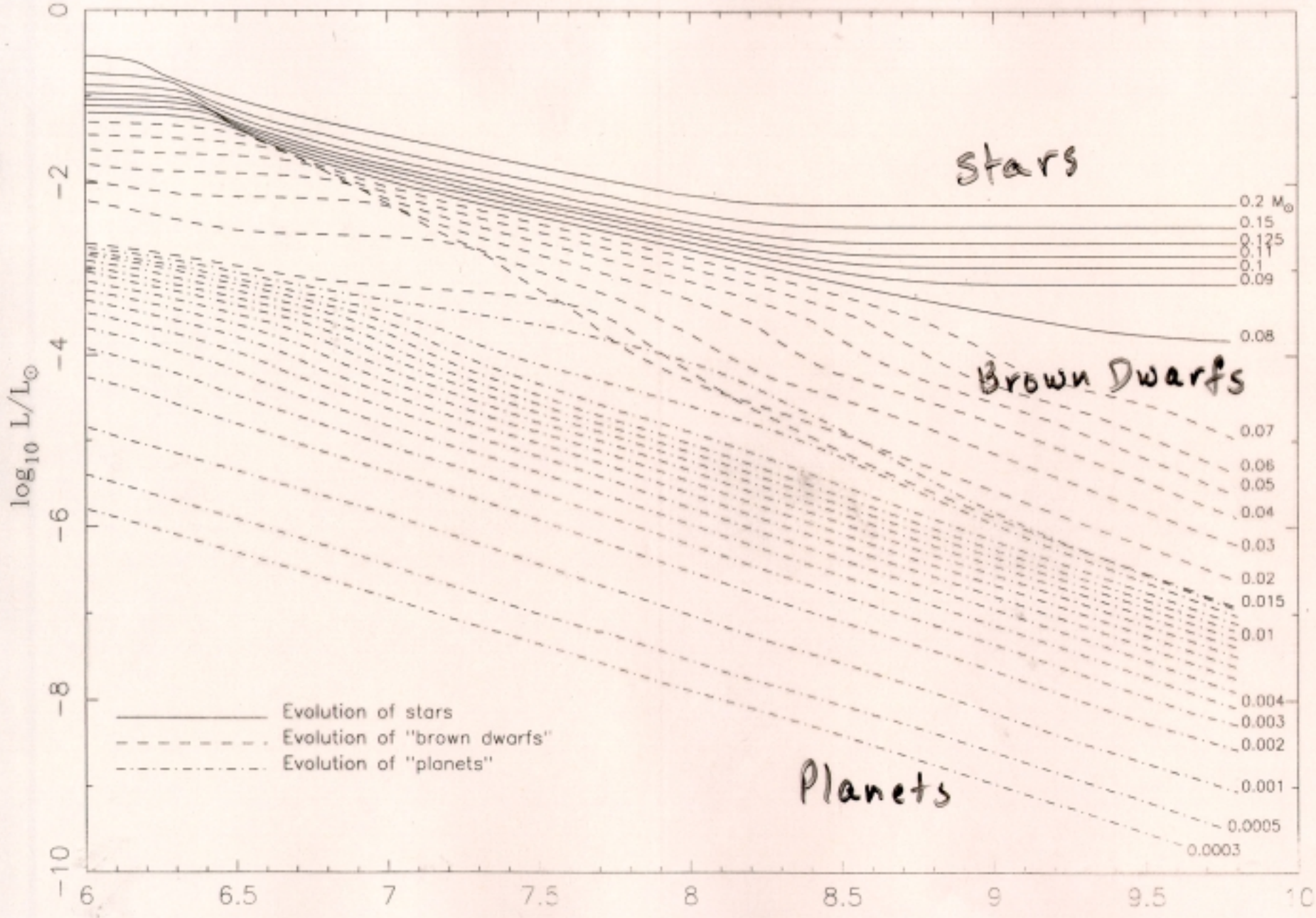

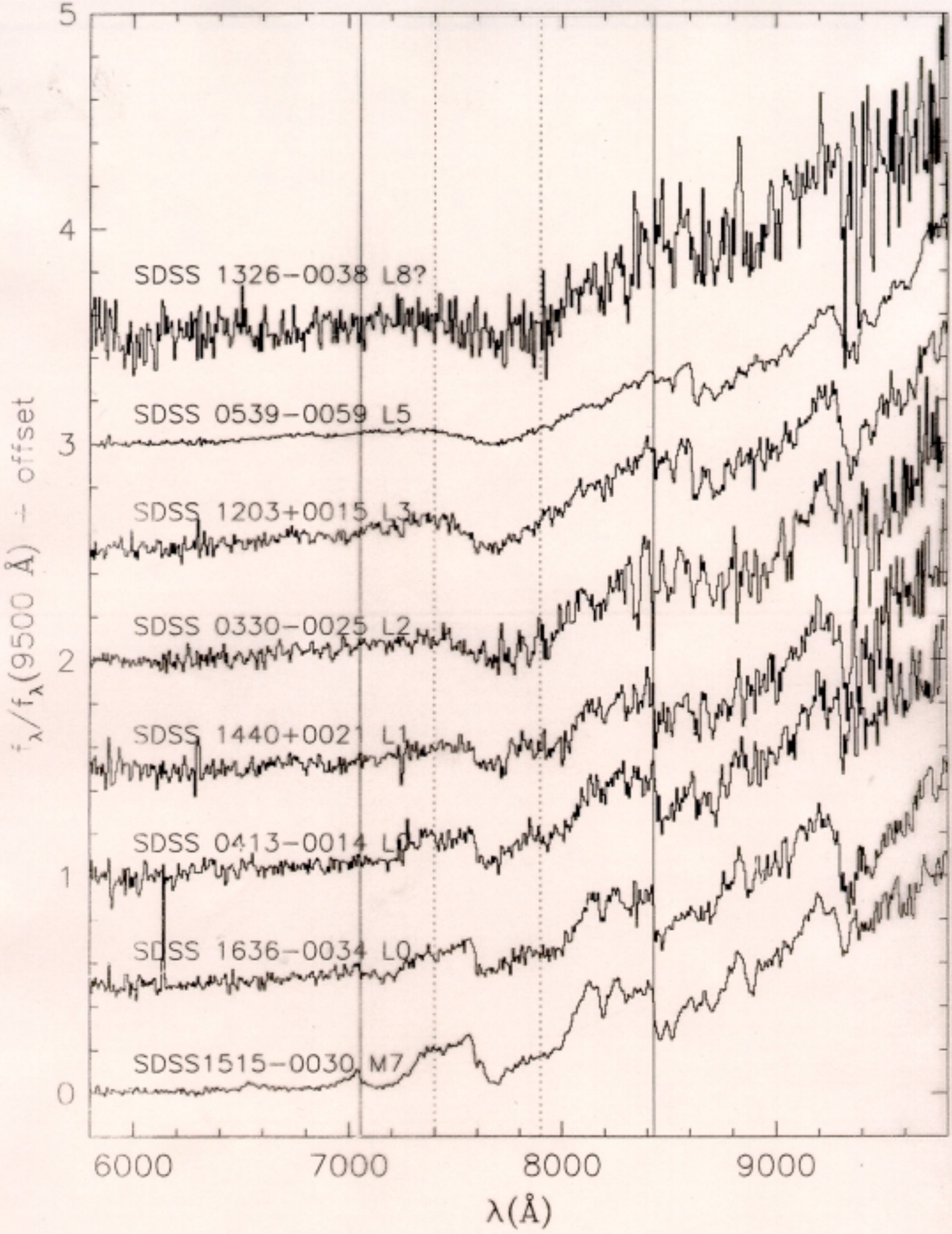
SDSS 1326−0038 L8?
SDSS 0539−0059 L5
SDSS 1203+0015 L3
SDSS 0330−0025 L2
SDSS 1440+0021 L1
SDSS 0413−0014 L0
SDSS 1636−0034 L0
SDSS1515−0030 M7
$f_\lambda/f_\lambda(9500\ \text{Å})$ + offset
λ(Å)
0
1
2
3
4
5
6000
7000
8000
9000

We have discovered objects with near-infrared spectra *intermediate* between L dwarfs and T dwarfs; showing both CH_4 and CO in their atmospheres. These cannot be distinguished from ordinary stars by their near-IR colors alone.

The challenges ahead:

- Determining accurate temperatures from the spectra.
- Measuring masses (use HST to find binary companions?).
- Measuring distances and thus luminosities.
- Determining their space density (comparable to main-sequence stars?).

Transition from L to T

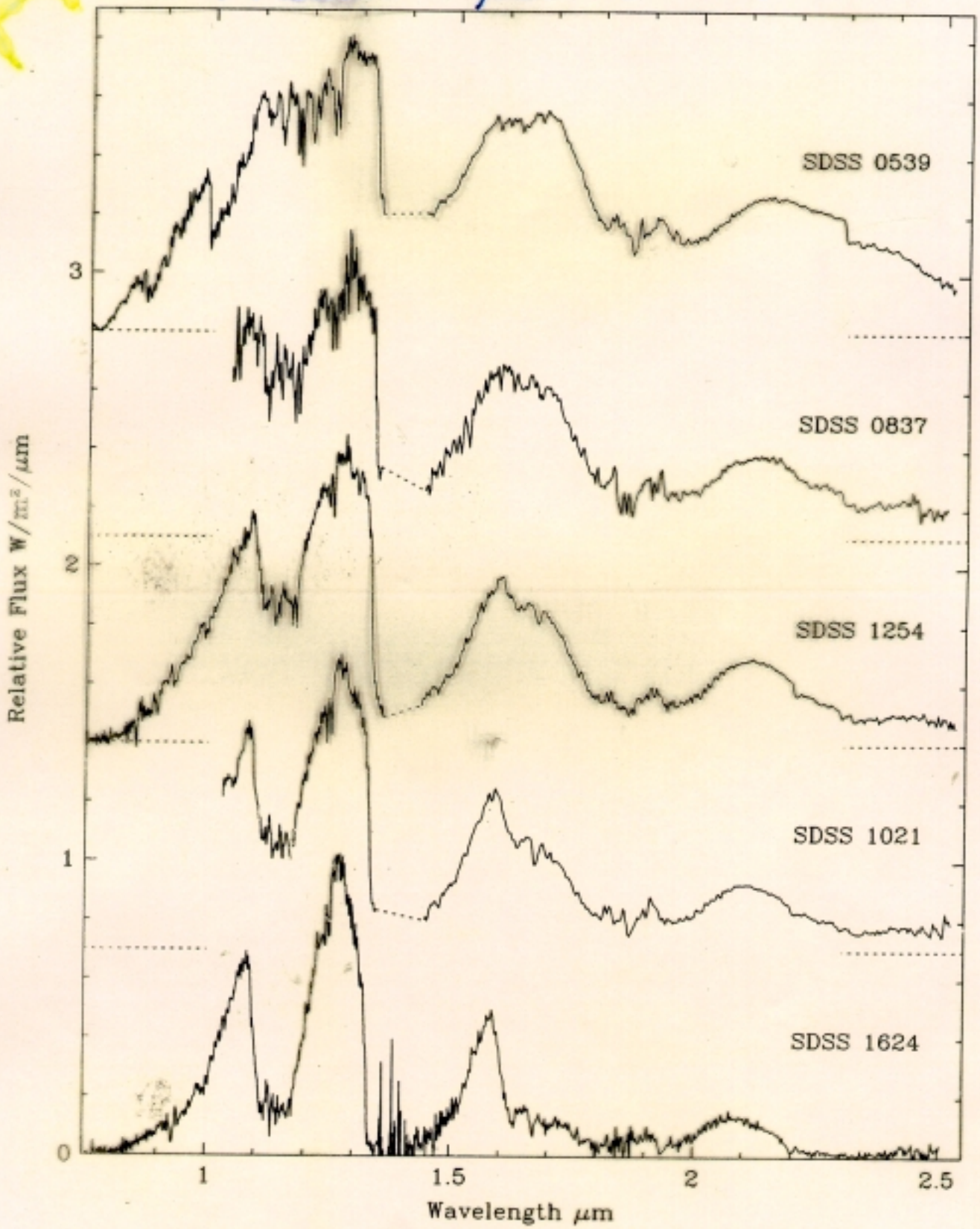

Kim, Nichol, Bahcall, Annis, Goto, Miller, McKay et al...

Clusters of Galaxies from SDSS Images

Clusters of galaxies are groupings of hundreds or thousands of galaxies within a few Megaparsec. They are often associated with hot gas (visible in X-rays), and large (> 1000 km/s) virial motions.

They are interesting:

- As laboratories to understand the formation and evolution of galaxies;
- As cosmological probes to the density field fluctuation spectrum;
- As laboratories to understand the distribution and nature of dark matter;
- Etc., etc.

They are rarely completely virialized; they show substructure, elongation, etc.

Not all astronomers agree on the formal definition of a cluster.

SDSS-2MASS overlap:

Color-color diagrams of stars.

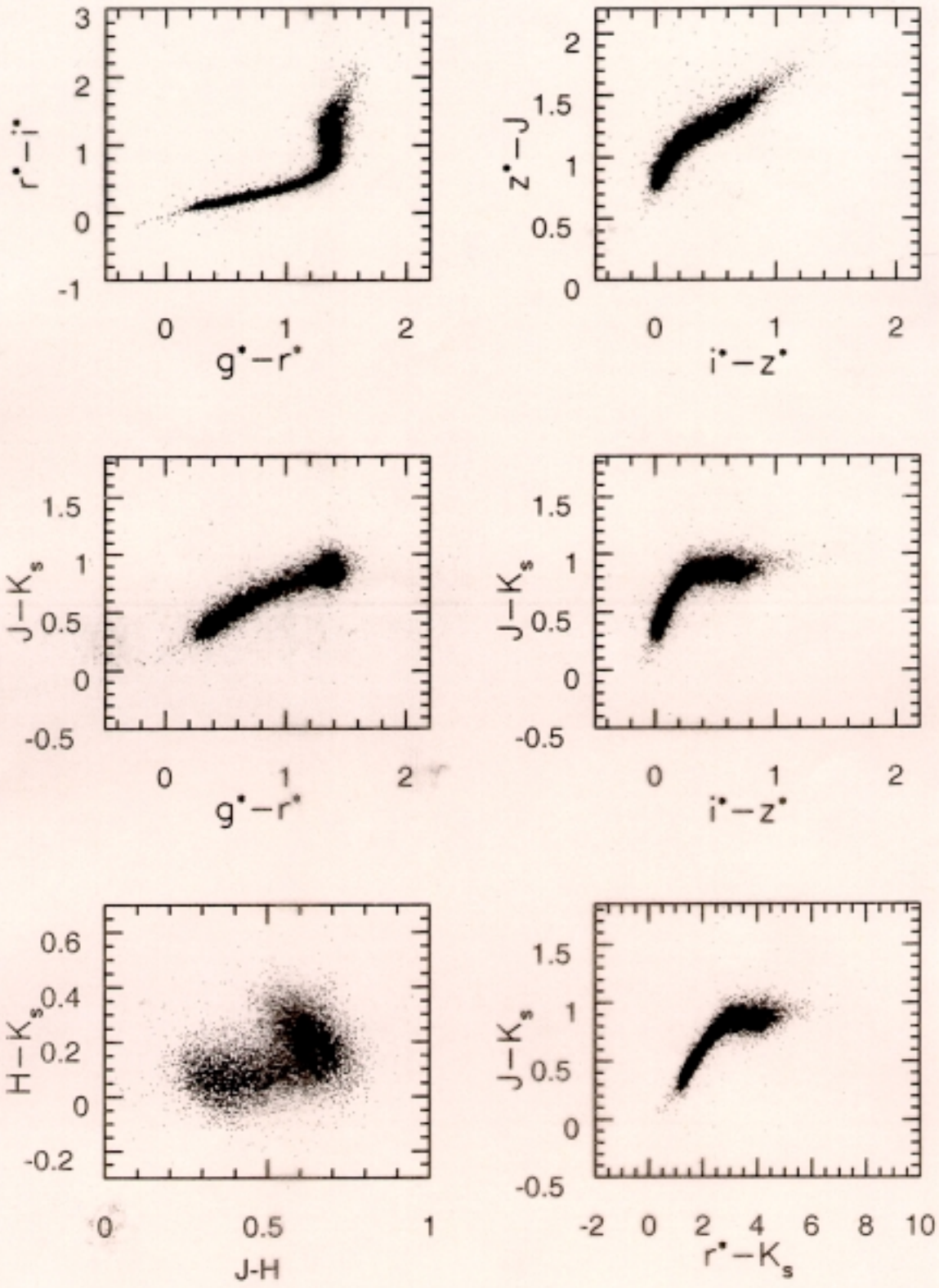

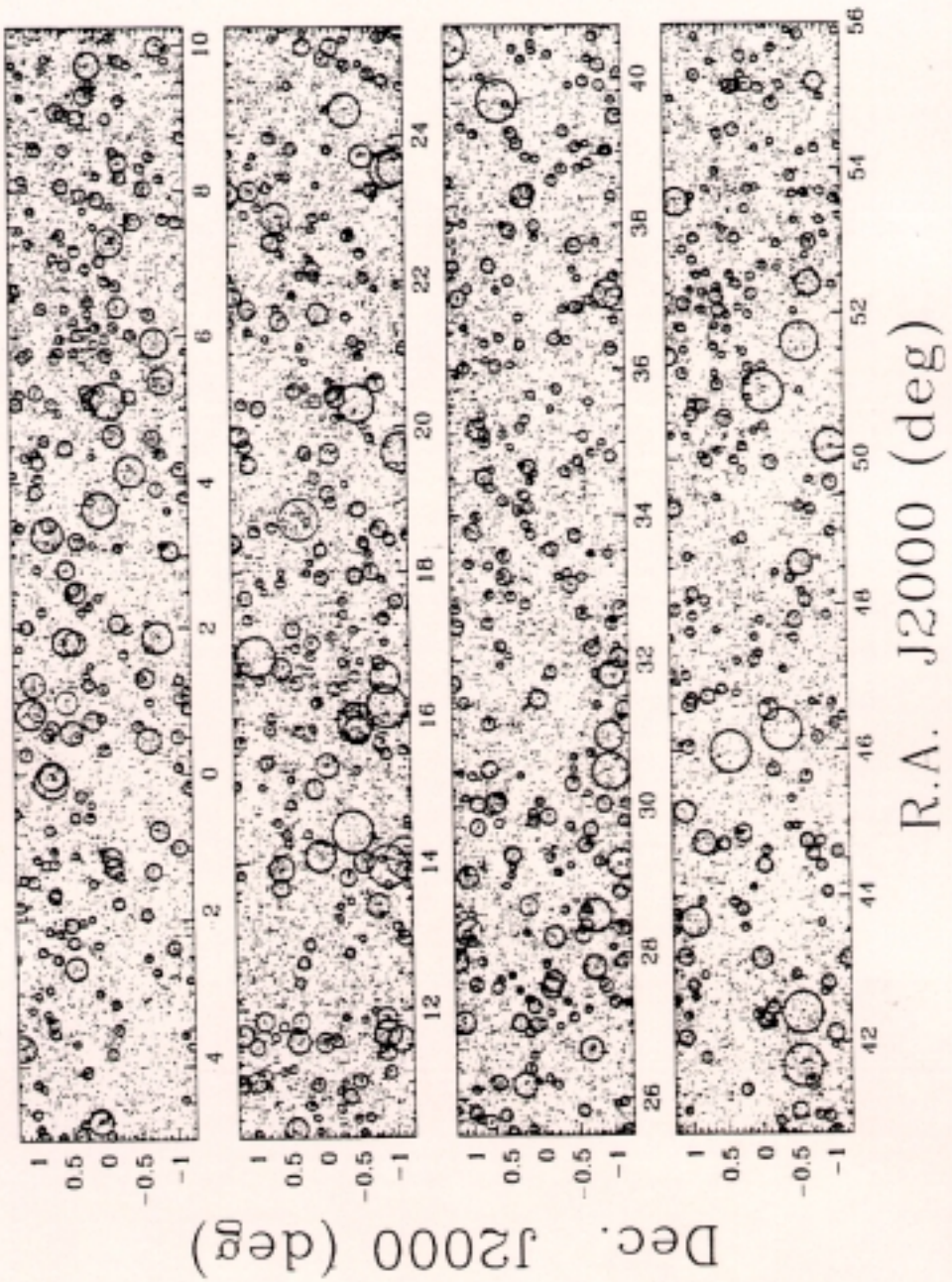

Figure 5.1: The distribution of 914 SDSS clusters in the SMV sample with positive visual identification (VC=1), plotted over the galaxy distribution ($r' \leq 20$). The radii of the circles are $1h^{-1}$ Mpc at the estimated cluster redshift. Abell Richness Class (RC) ≥ 1 (magenta) and RC $= 0$ (cyan) clusters are presented.

Color-magnitude diagrams show E-S0 ridgeline.

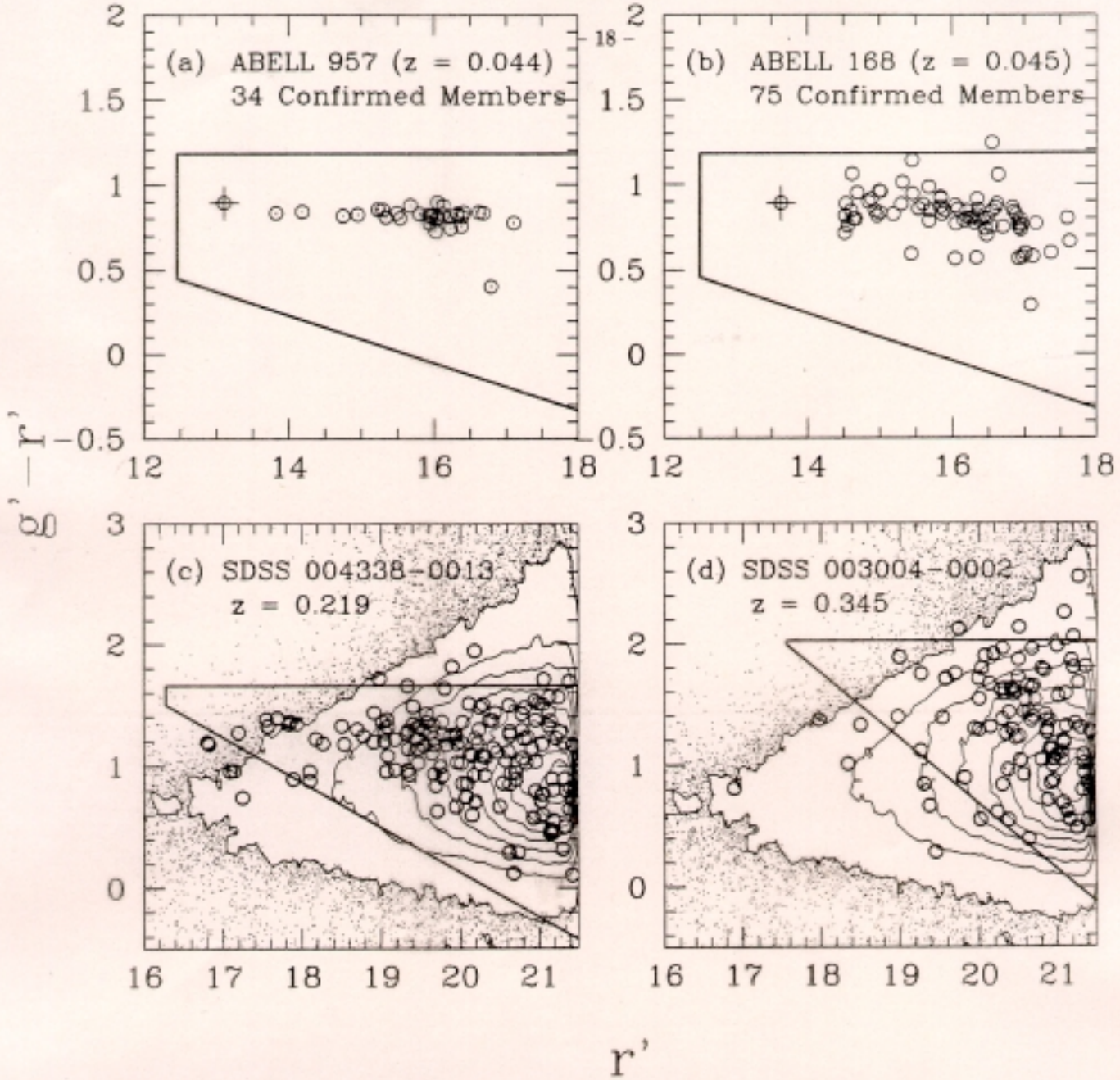

Fig. 1.— Color-magnitude (C-M) diagrams of four different clusters. (a) and (b) are known Abell clusters, and plotted here are the data from only those galaxies with confirmed membership according to the ENACS (Katgert *et al.* 1998). All data are taken from SDSS photometry. (c) and (d) show C-M diagrams of new clusters found in the SDSS itself by the matched filter techniques. Both clusters were confirmed visually through 3 color (g', r', i') composite images and their redshifts ($z = 0.219$ and $z = 0.345$) were obtained by the SDSS spectroscopic survey (York *et al.* 2000). The circles represent galaxies within 1 h_{70}^{-1}Mpc of the detected center ($r = 4.74'$ and $r = 3.45'$) and the contours represent the C-M distribution of all galaxies from a 25 deg^2 region around the cluster. The thick solid lines in all four panels show the C-M filtering for the VTT (see text) at the corresponding redshifts, enclosing the region which most cluster galaxies inhabit for a given redshift. $g' - r'$ colors are from model magnitudes and r' is in Petrosian magnitudes.

Data are consistent with constant number density to $z = 0.4$

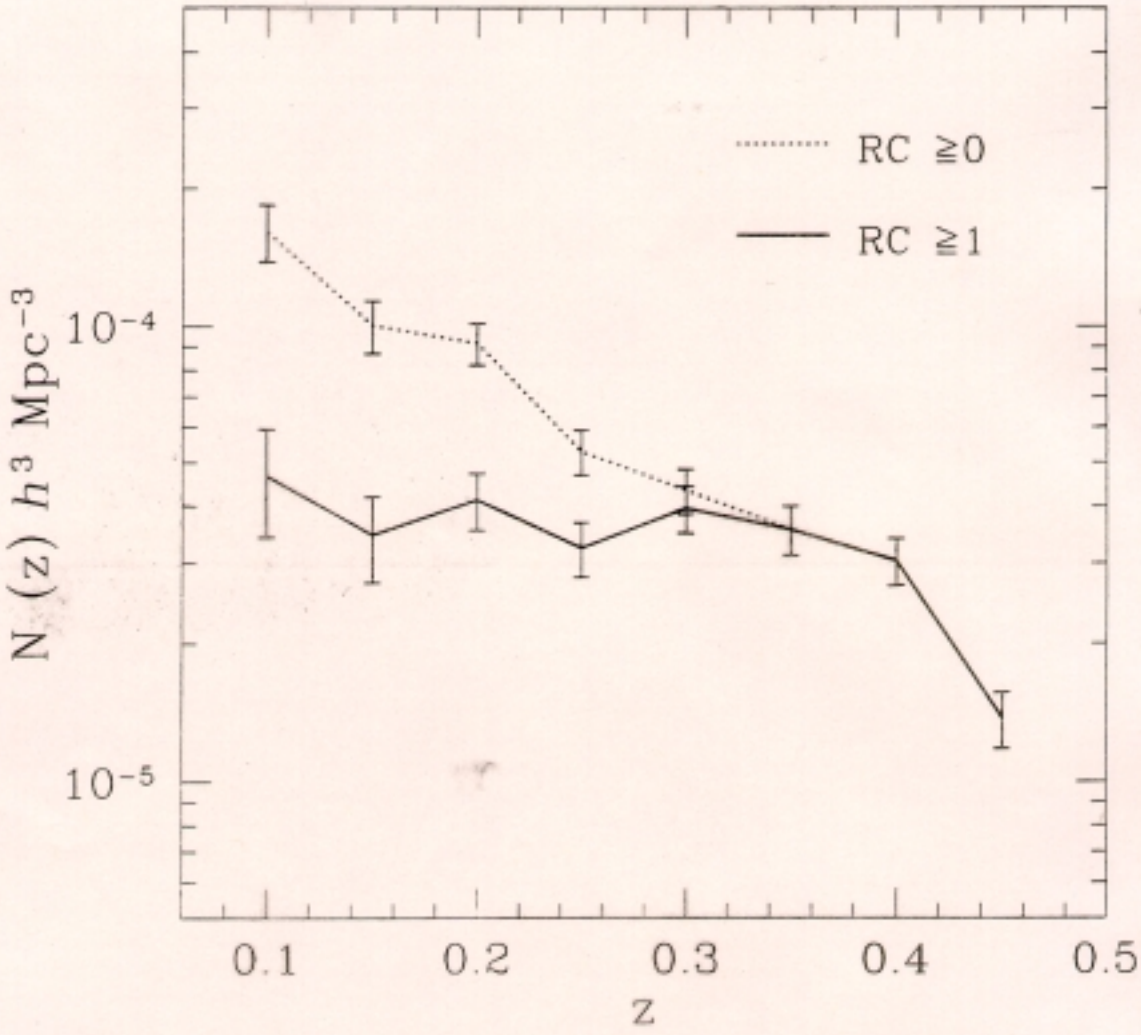

Figure 5.2: The cluster space density of SDSS clusters detected by the HMF as a function of redshift. Errorbars are from pure Poisson statistics. The division between RC = 0 and 1 is done by $\Lambda_{cl} = 33.3$. RC ≥ 1 clusters (solid line) show a remarkably constant comoving space density to $z \sim 0.4$, while RC ≥ 0 clusters (dotted line) show the effect of severe incompleteness or RC=0 clusters beyond $z \sim 0.2$. The average space density for RC ≥ 1 is $(3.5 \pm 0.2) \times 10^{-5}\, h^3 \mathrm{Mpc}^{-3}$.

Alignment of BCG with parent cluster.

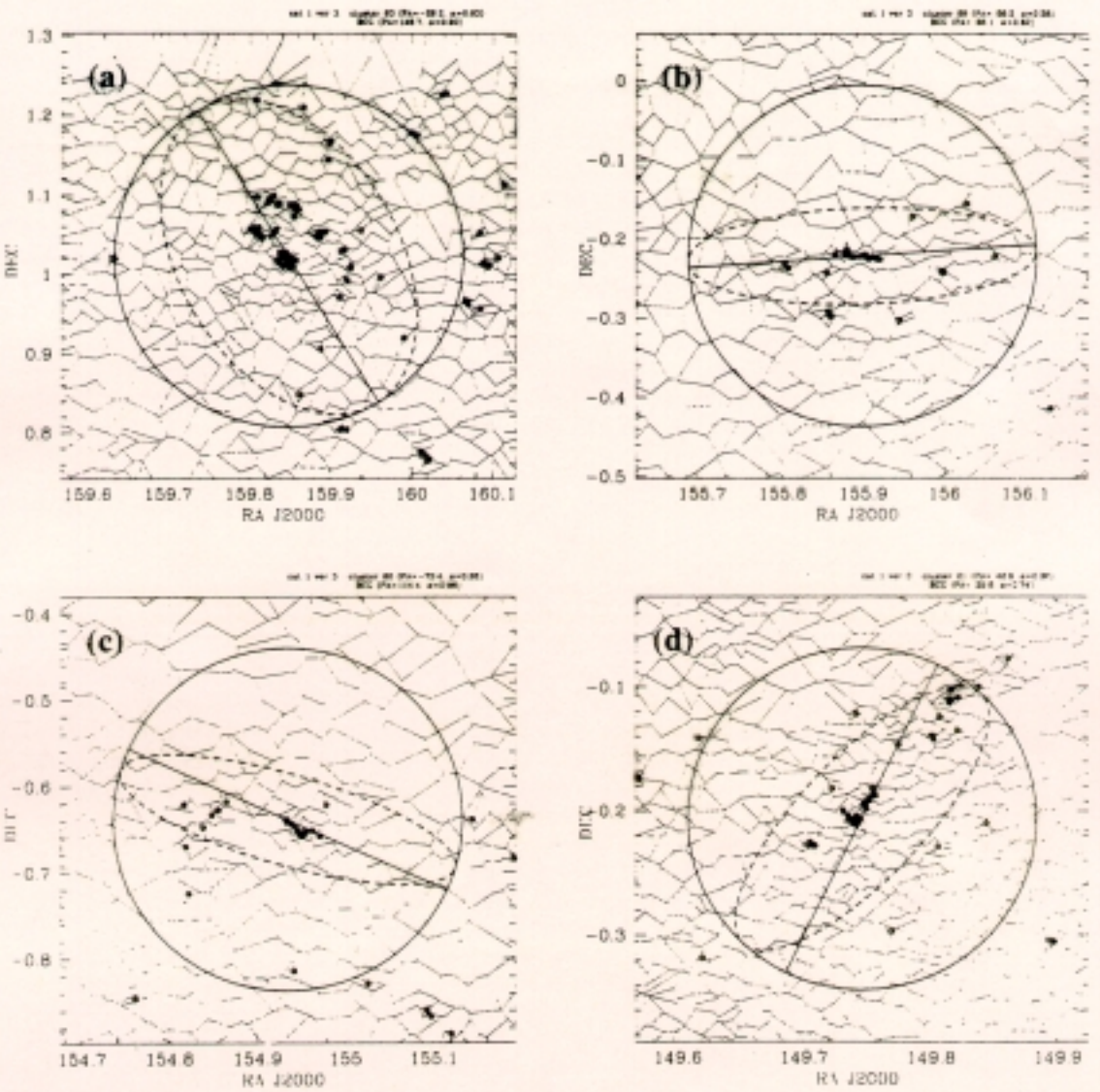

Fig. 8.— Illustration of cluster position angle determination and the alignment with its BCG. Each figure shows Voronoi Tessellation performed on galaxies that were selected through a color-magnitude filter at the cluster redshift. The resulting high density contrast ($\delta > 3$) galaxies are highlighted with red dots. with which we compute the cluster orientation (ϕ) and the axis ratio (α). The cluster ϕ and α are represented by an ellipse (blue-dashed) around the cluster center (BCG), with its major axis normalized to $1h^{-1}$ Mpc (solid circle). The green solid line represents the position angle of the BCG itself. Shown are four low redshift clusters with MaxBCG estimated redshifts: (a) $z = 0.1$ (b) $z = 0.1$ (c) $z = 0.11$ and (d) $z = 0.17$.

Clusters with dominant BCG

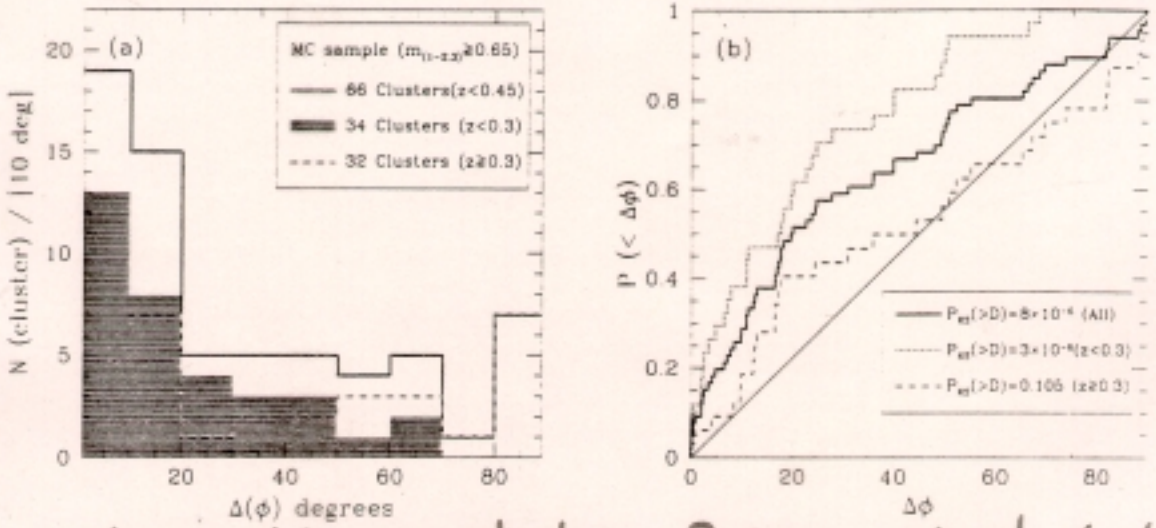

Angle difference between BCG and host cluster.

Fig. 15.— Same as Fig. 14, for a total of 66 Machine Confirmed (MC) clusters, that have dominant BCGs measured by the index $m_{(1-2.3)} \geq 0.65$, and bound by $z < 0.45$ (the redshift region where background contamination is small). The 34 low z clusters ($z < 0.3$) show striking alignment ($P_{KS}(> D) = 3 \times 10^{-6}$), while the 32 high z clusters ($0.3 \leq z < 0.45$) only show mild correlation (90%). However the overall signal (solid histogram, solid curve) is improved somewhat from the 88 VC sample shown in Fig. 14.

Clusters with less dominant BCG.

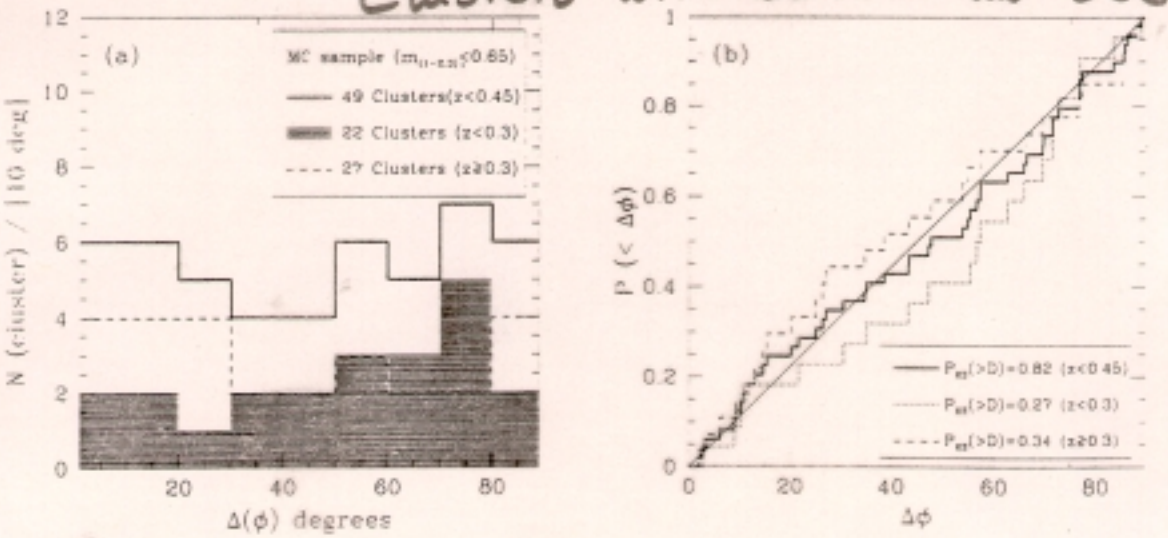

Fig. 16.— Same as Fig. 15, for a total of 49 clusters in the MC sample, with less dominant BCGs selected by $m_{(1-2.3)} < 0.65$, and $z < 0.45$. The distribution of these 49 clusters does not show any departure from randomness whatsoever ($P_{KS}(> D) = 0.82$). The low and high z subsamples are also consistent with a random distribution roughly within 1σ ($P_{KS}(> D) = 0.27$ and 0.34 for low z and high z, respectively).

Structure of the Galactic Halo

The halo of the Milky Way is a roughly spherical sprinkling of old stars. It has been suggested to have grown by accreting small neighboring galaxies. The remains of this "galactic cannibalism" might still be recognizable in the distribution of stars.

The challenge: look for coherent overdensities in the distribution of stars in position/color/magnitude space. These will likely be very extended over a large area of sky.

These "tidal streamers" have been seen in SDSS and other data. How can we make a complete catalog of them?

Looking for very nearby dwarf galaxies is a similar problem; they will appear as low-contrast overdensities in the stellar distribution, extended over tens of arcminutes.

Mixture models may be an effective way to find them.

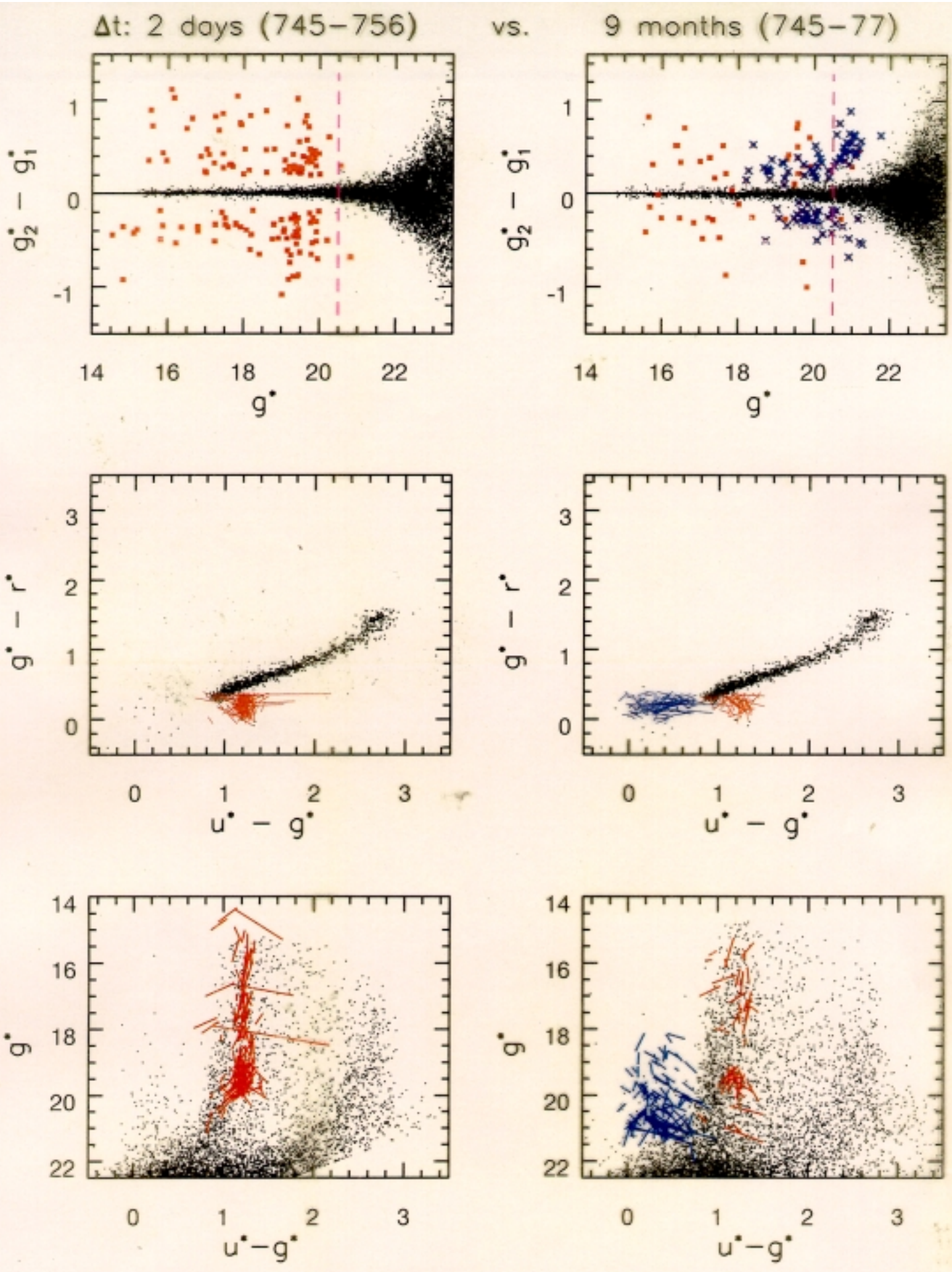
Δt: 2 days (745−756)
vs.
9 months (745−77)
$g_2^* - g_1^*$
g^*
$g^* - r^*$
$u^* - g^*$
g^*
$u^* - g^*$

RR Lyraes

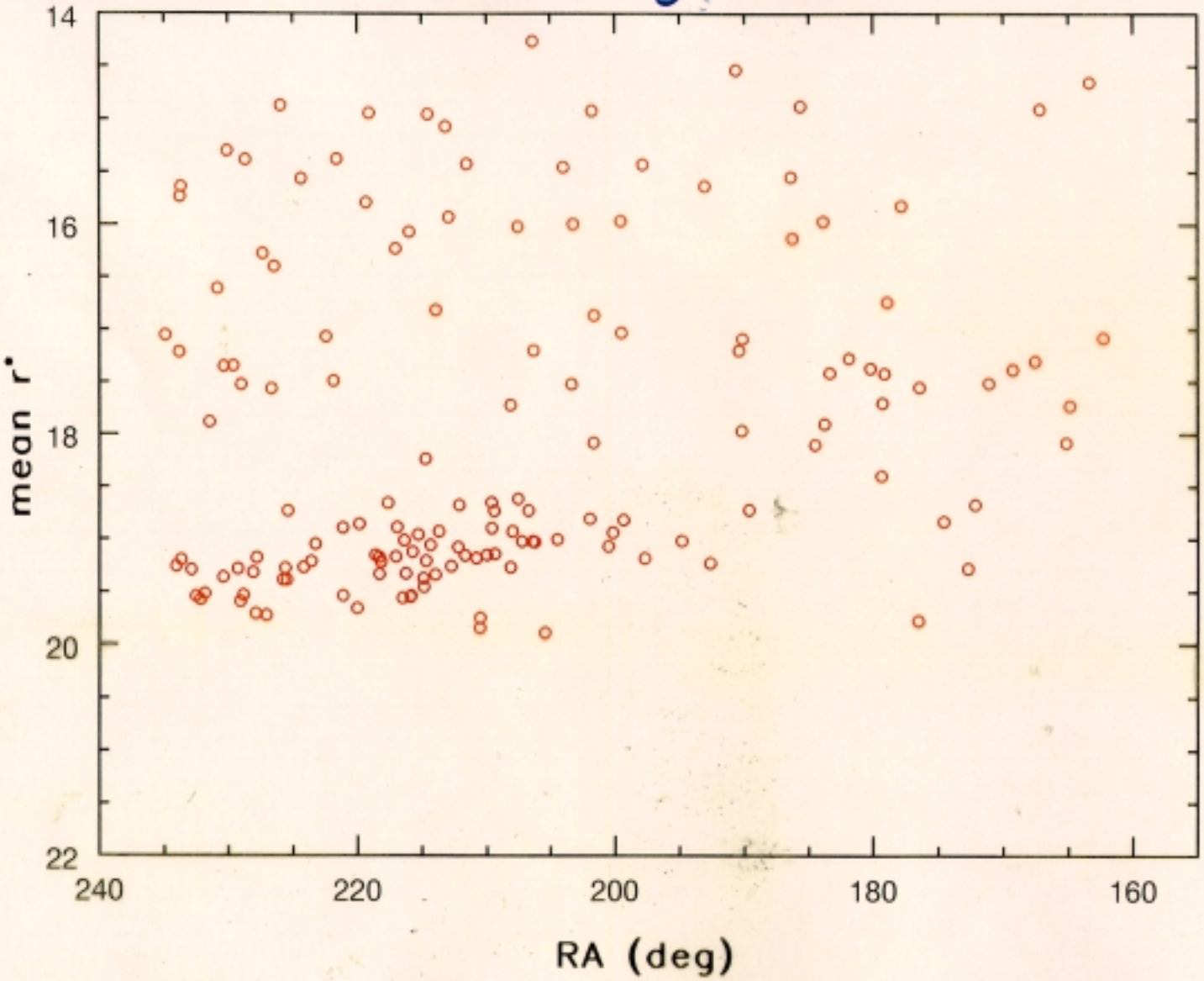

Newberg, Yanny et al.

Pal 5 shows tidal tails!

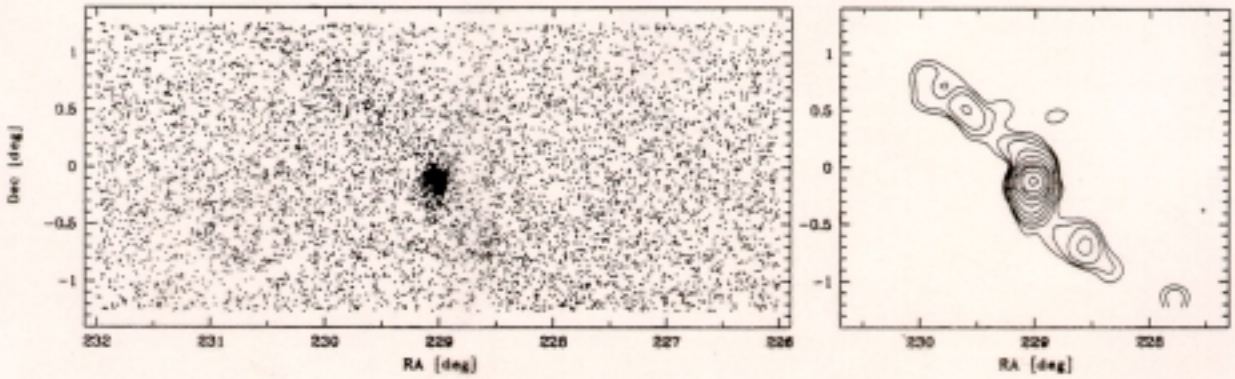

Fig. 2.— Projected spatial distribution of the photometric cluster member candidates selected with the method described in Section 2. Left: individual star positions. Right: contours of the surface density derived by adaptive kernel estimation. Contour levels are 0.19, 0.21, 0.24, 0.3, 0.4, 0.6, 1.0, 2.0, 4.0 and 8.0 stars/□′. The background has a mean of 0.13 stars/□′.

$u^* - g^*$, $i^* - z^*$, and c_2 according to the borders of the cluster population defined by stars from the cluster core ($r \leq 3'$), and according to the estimated spread due to photometric errors (for c_2 cf. leftmost panel of Fig. 1).

After this preselection, we used Grillmair's method for filtering in the color-magnitude plane of (c_1, i^*). The local signal-to-noise s of the expected true number of clusters stars was determined on a grid of mesh size 0.01 mag in c_1 and 0.05 mag in i^*. For each grid point (index k) the number $n_c(k)$ of stars in a circle of radius $12'$ around the cluster center and the number $n_f(k)$ of stars at more than 2° angular distance from the cluster center were counted in a color-magnitude box of width 0.09 mag in c_1 and 0.35 mag in i^* centered on that point. With n_c representing the number of cluster stars plus underlying field stars, n_f the number of field stars, and q the ratio of the areas on which n_f and n_c have been sampled, s was calculated as given by eq.(2).

$$s(k) = \frac{n_c(k) - q^{-1} n_f(k)}{\sqrt{n_c(k) + q^{-2} n_f(k)}} \qquad (2)$$

The size of the color-magnitude boxes and the overlap between boxes around neighboring grid points assure that s is a sufficiently smooth function. From the local signal-to-noise s one obtains a filtering mask in the (c_1, i^*) plane by setting a threshold $s_{lim} < s_{max}$ and by isolating the region in the grid (around the maximum of s) with $s \geq s_{lim}$. In order to find the most appropriate mask, we went through a series of gradually decreasing thresholds, counted for each threshold the cumulative number of stars in the corresponding mask in the area of the cluster's tails (N_t) and in the outer field (N_f), and determined from these numbers the cumulative signal-to-noise ratio SNR of the expected true number of cluster stars in the area of the tails (eq.(3)).

$$\mathrm{SNR} = \frac{N_t - w^{-1} N_f}{\sqrt{N_t + w^{-2} N_f}} \qquad (3)$$

The filtering mask was then chosen such that the cumulative signal-to noise reaches a maximum. As shown in Fig. 1 (second panel from left) this mask cuts out the zone from the bottom of the subgiant branch to the main-sequence turnoff and further down the main sequence to $i^* = 22.0$ mag. In the range $19.5 \leq i^* \leq 21.5$ the width of the mask approximately coincides with the 2σ limits for the dispersion of cluster stars in c_1 as derived from the median values of the estimated photometric errors. The two panels on the right in Fig. 1 give an example of the detection of cluster member candidates outside the cluster using the filter mask in the area of the cluster's tails and in the area of the outer field.

Oden Kirchen et al.

Conclusions

The Sloan Digital Sky Survey is underway. It is performing close to specifications, and will achieve its scientific goals.

There are already **many** more exciting science results than can be covered in a one-hour talk!

Among the most exciting science results are those things we did not anticipate doing with the SDSS:

- Brown dwarfs
- Structure of the halo from RR Lyrae stars
- Asteroid science
- Detection of the Gunn-Peterson effect
- Weak lensing studies and the masses of galaxies
- Tidal tails of globular clusters
- The discovery of very cool white dwarfs
- The discovery of extreme Broad Absorption Line quasars